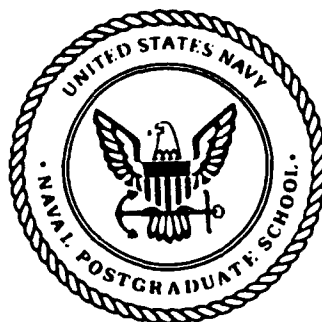


AD-A202 029

# NAVAL POSTGRADUATE SCHOOL Monterey, California

DTIC FILE COPY



## THESIS

DISCRETE PRECIPITATION EFFECTS ON SEA-  
SONAL MIXED LAYER DYNAMICS  
IN THE NORTH PACIFIC OCEAN

by

Mendal S. Livezey

September 1988

Thesis Advisor  
Co-Advisor

Roland W. Garwood  
Pecheng Chu

Approved for public release; distribution is unlimited.

DTIC  
ELECTE  
DEC 29 1988

S

D

H

*Handwritten signature*

331

Unclassified

security classification of this page

REPORT DOCUMENTATION PAGE				
1a Report Security Classification <b>Unclassified</b>			1b Restrictive Markings	
2a Security Classification Authority			3 Distribution Availability of Report	
2b Declassification Downgrading Schedule			Approved for public release; distribution is unlimited.	
4 Performing Organization Report Number(s)			5 Monitoring Organization Report Number(s)	
6a Name of Performing Organization Naval Postgraduate School		6b Office Symbol (if applicable) <b>68Gd</b>	7a Name of Monitoring Organization Naval Postgraduate School	
6c Address (city, state, and ZIP code) Monterey, CA 93943-5000			7b Address (city, state, and ZIP code) Monterey, CA 93943-5000	
8a Name of Funding Sponsoring Organization		8b Office Symbol (if applicable)	9 Procurement Instrument Identification Number	
8c Address (city, state, and ZIP code)			10 Source of Funding Numbers	
			Program Element No	Project No
			Task No	Work Unit Accession No
11 Title (include security classification) <b>DISCRETE PRECIPITATION EFFECTS ON SEASONAL MIXED LAYER DYNAMICS IN THE NORTH PACIFIC OCEAN</b>				
12 Personal Author(s) <b>Mendal S. Livezey</b>				
13a Type of Report Master's Thesis		13b Time Covered From To	14 Date of Report (year, month, day) September 1988	15 Page Count 80
16 Supplementary Notation The views expressed in this thesis are those of the author and do not reflect the official policy or position of the Department of Defense or the U.S. Government.				
17 Cosati Codes			18 Subject Terms (continue on reverse if necessary and identify by block number)	
Field	Group	Subgroup	Oceanography, Air-Sea Interaction, Mixed Layer Modeling	
			7	
19 Abstract (continue on reverse if necessary and identify by block number)				
<p>This study was conducted to examine the effects of discrete precipitation events on the short-term and seasonal evolution of ocean mixed layer temperature and salinity structure. This study was located at Ocean Station "P" (50°N, 145°W) in the Northeast Pacific Ocean. Two numerical modeling experiments were performed. The first was to simulate the response of the mixed layer to hypothetical discrete (isolated) precipitation events. This experiment showed that the effect of a single discrete rain event can vary with season, with the mixed layer depth (MLD) at onset of the rain event, and with the strength of wind stress forcing. A single rain event can have lasting effects on mixed layer depth and temperature for up to 55 days after the event, depending upon the season.</p> <p>The second experiment simulated quasi-realistic "complex" precipitation forcing, with a realistic distribution of synoptic events over a 13-month period. For this experiment, four different precipitation "intensities" were tested. The values of temperature, salinity, and MLD predicted by the model were compared with observed Conductivity Temperature Depth measurements and with the values predicted using constant precipitation forcing. In all experiments, the modelled MLD's approximated the observed MLD and temperature cycle. MLD's for all cases were too deep while temperature was estimated well in winter and was too cool in summer. Predicted salinity provided the greatest discrepancy between the modeled and the observed cycle. The 96 cm/400-day quasi-realistic precipitation-forced case best approximated the salinity observations though predicted salinity was fresher than observed in winter and saltier than observed in summer. Model results suggest that the amount of precipitation observed at Ocean Station "P" was too low to explain the observed and simulated ocean salinity and temperature structure for the year.</p>				
20 Distribution Availability of Abstract			21 Abstract Security Classification	
<input checked="" type="checkbox"/> unclassified unlimited <input type="checkbox"/> same as report <input type="checkbox"/> DTIC users			Unclassified	
22a Name of Responsible Individual Rowland W. Garwood			22b Telephone (include Area code) (408) 646-3260	22c Office Symbol <b>68Gd</b>

DD FORM 1473,84 MAR

83 APR edition may be used until exhausted  
All other editions are obsolete

security classification of this page

Unclassified

Approved for public release; distribution is unlimited.

Discrete Precipitation Effects on Seasonal Mixed Layer Dynamics  
in the North Pacific Ocean

by

Mendal S. Livezey  
Lieutenant, United States Navy  
B.S., Indiana University, 1981

Submitted in partial fulfillment of the  
requirements for the degree of

MASTER OF SCIENCE IN METEOROLOGY AND OCEANOGRAPHY

from the

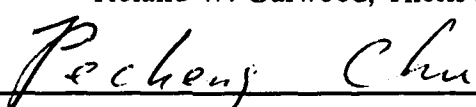
NAVAL POSTGRADUATE SCHOOL  
September 1988


Author:

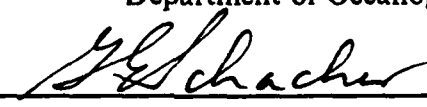
  
Mendal S. Livezey

Approved by:

  
Roland W. Garwood, Thesis Advisor

  
Peoheng Chu, Co-Advisor

  
Curtis A. Collins, Chairman,  
Department of Oceanography

  
Gordon E. Schacher,  
Dean of Science and Engineering

## ABSTRACT

This study was conducted to examine the effects of discrete precipitation events on the short-term and seasonal evolution of ocean mixed layer temperature and salinity structure. This study was located at Ocean Station "P" (50°N, 145°W) in the Northeast Pacific Ocean. Two numerical modeling experiments were performed. The first was to simulate the response of the mixed layer to hypothetical discrete (isolated) precipitation events. This experiment showed that the effect of a single discrete rain event can vary with season, with the mixed layer depth (MLD) at onset of the rain event, and with the strength of wind stress forcing. A single rain event can have lasting effects on mixed layer depth and temperature for up to 55 days after the event, depending upon the season.

The second experiment simulated quasi-realistic "complex" precipitation forcing, with a realistic distribution of synoptic events over a 13-month period. For this experiment, four different precipitation "intensities" were tested. The values of temperature, salinity, and MLD predicted by the model were compared with observed Conductivity Temperature Depth measurements and with the values predicted using constant precipitation forcing. In all experiments, the modelled MLD's approximated the observed MLD and temperature cycle. MLD's for all cases were too deep while temperature was estimated well in winter and was too cool in summer. Predicted salinity provided the greatest discrepancy between the modeled and the observed cycle. The 96 cm/400-day quasi-realistic precipitation forced case best approximated the salinity observations though predicted salinity was fresher than observed in winter and saltier than observed in summer. Model results suggest that the amount of precipitation observed at Ocean Station "P" was too low to explain the observed and simulated ocean salinity and temperature structure for the year.

Accession For	
NTIS GRA&I	<input checked="checked" type="checkbox"/>
DTIC TAB	<input type="checkbox"/>
Unannounced	<input type="checkbox"/>
Justification	
By _____	
Distribution/	
Availability Codes	
Dist	Avail and/or Special
A-1	

## TABLE OF CONTENTS

I. INTRODUCTION .....	1
A. LITERATURE REVIEW .....	1
B. RESEARCH PLAN: LOCATION AND PERIOD OF STUDY .....	4
II. DATA SOURCES AND PREPARATION .....	10
A. DATA SOURCES .....	10
B. VERTICAL INTERPOLATION .....	10
III. THEORY .....	12
A. OCEANIC MIXED LAYER STRUCTURE .....	12
B. ENTRAINMENT .....	12
C. MIXED LAYER THERMODYNAMICS: TEMPERATURE AND SALINITY BUDGETS .....	17
D. SALINITY EFFECT ON MIXED LAYER DYNAMICS .....	19
1. The Shallowing Effect .....	19
2. The Deepening Effect .....	20
IV. HYPOTHETICAL EXPERIMENTS .....	21
A. EFFECTS OF DISCRETE PRECIPITATION EVENTS .....	21
B. ANALYSIS OF PRECIPITATION EVENT EFFECTS .....	25
1. Event #1 (Dec 1968) .....	25
2. Event #2 (Jan 1969) .....	27
3. Event #3 (Feb 1969) .....	28
4. Event #4 (Mar 1969) .....	29
5. Event #5 (Apr 1969) .....	31
6. Event #6 (May 1969) .....	33
7. Event #7 (Jun 1969) .....	33
8. Event #8 (Jul 1969) .....	35
9. Event #9 (Aug 1969) .....	37
10. Event #10 (Sep 1969) .....	37
11. Event #11 (Oct 1969) .....	39

12. Event #12 (Nov 1969) .....	39
C. EXPERIMENT SUMMARY .....	39
V. PROCEDURES, RESULTS, AND ANALYSIS .....	41
A. PROCEDURES .....	41
B. RESULTS AND ANALYSIS .....	45
1. Complex Precipitation and Evaporation Forcing .....	45
2. Constant Precipitation and Evaporation Forcing .....	55
VI. SUMMARY .....	63
REFERENCES .....	67
INITIAL DISTRIBUTION LIST .....	69

## LIST OF FIGURES

Fig. 1. Region Surrounding Ocean Station "P" (from Tabata, 1961) . . . . .	6
Fig. 2. Oceanic Regime at Station "P." (from Favorite, 1976) . . . . .	7
Fig. 3. Example Temperature and Salinity Profiles . . . . .	8
Fig. 4. Example Temperature Profile . . . . .	13
Fig. 5. Example Salinity Profile . . . . .	14
Fig. 6. Conglomeration of Six Events (Dec 1968 to May 1969) . . . . .	22
Fig. 7. Conglomeration of Six Events (Jun to Nov 1969) . . . . .	23
Fig. 8. Event #1 (Dec 1968) . . . . .	26
Fig. 9. Event #4 (Mar 1969) . . . . .	30
Fig. 10. Event #5 (Apr 1969) . . . . .	32
Fig. 11. Event #7 (Jun 1968) . . . . .	34
Fig. 12. Event #8 (Jul 1968) . . . . .	36
Fig. 13. Event #10 (Sep 1969) . . . . .	38
Fig. 14. Front and associated wind directions and isotherms . . . . .	42
Fig. 15. Complex Rain Model Output and Winds for 400 day period . . . . .	43
Fig. 16. Simple and Complex Precipitation Forcing . . . . .	46
Fig. 17. Complex Precipitation Forcing Predicted MLD's . . . . .	47
Fig. 18. Subtracted Values of Complex Precipitation Forcing Output . . . . .	48
Fig. 19. Complex Precipitation Forcing Predicted Temperatures . . . . .	49
Fig. 20. Complex Precipitation Forcing Predicted Salinities . . . . .	51
Fig. 21. Complex Precipitation Forcing Predicted MLD and CTD MLD . . . . .	52
Fig. 22. Complex Precipitation Forcing Predicted and CTD Temperature . . . . .	53
Fig. 23. Complex Precipitation Forcing Predicted and CTD Salinity . . . . .	54
Fig. 24. Simple Precipitation Forcing Predicted MLD'S . . . . .	56
Fig. 25. Simple Precipitation Forcing Predicted Temperature . . . . .	57
Fig. 26. Simple Precipitation Forcing Predicted Salinity . . . . .	59
Fig. 27. Subtracted Mixed Layer Values From High Complex and Simple Cases . . . . .	60
Fig. 28. Simple, Complex, and Actual Mixed Layer Values . . . . .	61

## ACKNOWLEDGEMENTS

I would especially like to thank Dr. Roland W. Garwood for his encouragement throughout this thesis study, and to Dr. Pecheng Chu whose door was open for my "unending questions." Their enthusiasm and confidence in me and in the worthiness of this project was unflagging. Dr. Susuma Tabata at the Institute of Ocean Sciences, Sydney, British Columbia, Canada graciously provided me with background material and advice, for which I am grateful. And to my wife, I offer my heartfelt thanks for her enduring patience and understanding.



## I. INTRODUCTION

Salinity in the oceanic mixed layer and its change in depth with time can have a significant impact on upper ocean dynamics. Alterations of upper ocean salinity caused by precipitation and evaporation through buoyancy fluxes may also change the temperature profile of the ocean, altering the sound velocity. The purpose of this study was to examine the effects of discrete precipitation events on the evolution of the mixed layer depth (MLD) at Ocean Station "P" (50°N, 145°W).

Previous one-dimensional mixed layer prediction experiments had failed to accurately explain and predict the behavior of salinity with time and depth. Possible reasons for this were:

1. the amount of precipitation and evaporation was incorrectly specified,
2. the precipitation and evaporation distribution with time, relative to wind events was incorrectly specified, and or
3. the advection was incorrectly specified or neglected.

This study focused specifically on the variation of precipitation and evaporation with time. The total amounts of precipitation and evaporation are also varied. Possible effects of advection are discussed.

### A. LITERATURE REVIEW

Kraus and Turner (1967) provided the fundamental turbulent kinetic energy (TKE) theory on which many subsequent oceanic mixed layer models are based. This model considered the turbulent kinetic energy equation in a one-dimensional mixed layer scheme, using the approximately decoupled state of the mechanical and thermal energy equations. It was assumed that the heat input at the air-sea interface and the mass entrainment at the base of the mixed layer were uniform throughout the mixed layer for short time scales. Wind stress effects on the air-sea interface acted to increase the potential energy in the mixed layer by generating turbulent kinetic energy for mixing and entrainment. Entrainment was considered to be proportional to the wind energy input to the water column minus the work performed in overcoming the buoyant forces throughout the mixed layer. This type of turbulent erosion modeling considered buoyancy and wind forcing only, and it neglected viscous dissipation. This neglect of

dissipation has generally been considered a serious flaw. Kraus and Turner (1967) did not consider salinity effects in their mixed layer model.

Subsequent works, such as Geisler and Kraus (1969), Miropol'skiy (1970), and Denman (1973) have attempted to consider dissipation by assuming dissipation to be a fixed portion of wind stress. The Denman (1973) model was used in the first mixed layer simulation experiment to use Ocean Station "P" data (Denman and Miyake, 1973).

Miller (1976) was the first to include salinity and its effects on the density structure in a mixed layer model. Miller modified Denman (1973) to include salinity and used data from BOMEX Period III upper ocean soundings for periods of as long as 10 days for forcing and initial conditions. Four specific cases were examined by selecting distinctly different initial conditions for the salinity and temperature profiles and forcing data from BOMEX surface observations. In three cases, Miller examined the effects of three different initial conditions while the fourth case included a precipitation event.

The Miller study indicated that mixed layer salinity greater than the salinity of the water below the mixed layer may cause convective overturning due to density instability unless a sufficiently large temperature decrease occurred simultaneously across the interface. A large density jump across the interface acted to slow the mixed layer deepening rate due to an increase in potential energy. Without entrainment salinity flux effects, the cooling induced by entrainment was greater than the heating from the surface, resulting in net mixed layer cooling. With salinity included in the model, the layer deepened more slowly and entrained less cold water at the bottom, allowing surface heating to dominate and, therefore, the mixed layer temperature to increase. Overall, the results of these cases demonstrated the importance of salinity fluxes and the need to include the salinity profile in the prediction of mixed layer deepening and resultant temperature structure.

Miller demonstrated the potential significance of precipitation episodes in mixed layer modeling in a fourth case. His study demonstrated that precipitation can contribute to salinity fluxes within the mixed layer. However, the fact that salinity regularly fluctuates by  $\pm 0.15\%$  (due to horizontal advection) makes decreases in salinity due to rainfall difficult to detect in observations. Though Miller admittedly did not understand the nature of the effects of rainfall on the mixed layer, he did propose that even minor changes in the salinity flux due to precipitation may have a long term effect on the mixed layer thermal structure.

Paulus (1978) examined the effects of a salinity profile on density structure using a modified version of the Camp (1976) one-dimensional mixed layer model. The effects of a surface salinity flux on the mixed layer were examined using a constant evaporation and precipitation rate. Model initialization was accomplished with hydrocast data or XBT data with historical salinity profiles adjusted to realistically correspond to the temperature profiles. The incorporation of observed salinity profiles into the model had little effect on sea surface temperature (SST) and MLD during the summer regime (when MLD was shallow). However, when using the same forcing conditions for the winter regime the inclusion of a salinity profile acted to produce a warmer, shallower mixed layer than obtained when density was only a function of temperature.

Paulus suggested that the retreat of the isothermal layer could be enhanced due to precipitation by slowing the deepening rate and shoaling tendency of the mixed layer under downward heat flux. With respect to salinity flux, Paulus concluded that imbalances in evaporation and precipitation had more pronounced effects on SST and MLD in the long term than in the short term. His study concluded that this was a cumulative effect. Therefore, Paulus concluded that the addition of salinity effects to the mixed layer model was desirable.

Garwood (1977) introduced a one-dimensional bulk model of the oceanic mixed layer that included dynamic instability with turbulent erosion. This model modulated the mean entrainment rate by diurnal heating and limited maximum layer depth by enhancing the effect of viscous dissipation. This allowed a cyclic steady state to occur over an annual time period. It recognized the important effects of long term salinity fluxes on the mixed layer thermal profile due to surface heat fluxes, precipitation, and entrainment at the base of the mixed layer. This was the model of choice for this study.

Garzon (1987) used an oceanic mixed layer model to determine the specific effects of fresh water flux on the seasonal pycnocline in the mixed layer at Ocean Station "P." First, sensitivity of the model proposed by Garwood (1977) was examined by performing a hypothetical experiment using constant forcing with a wide range of precipitation and evaporation values. These results were compared to an identical model run with  $P-E$  (precipitation minus evaporation) = 0.0. This simple hypothetical case examined the relative importance of excess evaporation or precipitation over a time period of one-year. For the case with excess precipitation, a reduction in downward buoyancy and a decrease in surface salinity occurred, resulting in a shallower MLD than would be expected if  $P-E=0$ . For the case with excess evaporation, an increase in downward

buoyancy flux and an increase in surface salinity occurred. This yielded a deeper MLD than would occur with  $P-E = 0$ .

For the annual simulation at Ocean Station "P," Garzon, using data from 1967, modeled temperature and salinity profiles with  $P-E = 0.0\text{m year}$ ,  $P-E = 0.5\text{m year}$ , and for monthly representative values of precipitation. Overall, MLD and surface salinity from the model well approximated those of the actual data. However, near the end of the study period, MLD and salinity values demonstrated increasing error particularly in approximating significant anomalous "spikes." Garzon suggested that a more realistic representation of discrete precipitation and evaporation events would result in more accurate model output, especially for the long term. Additionally, Garzon adjusted model output for advection of salinity by subtracting the linear fit from the predicted salinity time series.

Precipitation and evaporation events have been demonstrated to have a significant impact on mixed layer depth on both short and long time scales. These factors can act alone or may be coupled with such events as synoptic scale storms to modify the effects of these events. On a short time scale, daytime heating tended to cause shallowing of the oceanic mixed layer due to heating of the mixed layer despite the occurrence of evaporation which tended to promote deepening. Upward heat flux broke down the mixed layer causing deepening. Precipitation during this time period promoted shallowing, thus opposing this effect. These diurnal changes in mixed layer depth were moderated by annual effects that were associated with the annual radiation cycle. Strong winds, often associated with large scale synoptic events, when combined with low insolation values in winter, yielded deep mixed layer depths. However, precipitation events often accompanying these winds acted to lessen the effects of winds and were associated with discrete shallowing episodes that last for short periods of time. These effects were cumulative. Just as a reduction or increase in wind speed in winter yielded a substantially shallower or deeper mixed layer depth in summer, a reduction or increase of rain during the same period yielded a deeper or shallower mixed layer depth in summer.

## **B. RESEARCH PLAN: LOCATION AND PERIOD OF STUDY**

For this study, a time period was chosen to provide the best overlap of available data bases. The starting date of 23 November 1968 with a study period of 400-days was selected for this study, since it provided data base overlap, that is, surface forcing and

CTD data was available for this time period. This numerical simulation of 400-days used a time step of one hour.

The study area was between  $49^{\circ}$  N and  $51^{\circ}$  N, and  $144^{\circ}$  W and  $146^{\circ}$  W centered at Ocean Station "P" (Fig. 1 on page 6). From 1949 to 1981 the waters around Ocean Station "P" have been occupied by ocean station vessels year-round. This provided numerous data bases, such as, XBT, CTD, and atmospheric observations for analysis.

Tabata (1961,1965) described oceanographic and meteorological conditions at Station "P" in detail. The dominate pressure systems located in the North Pacific Ocean are the low pressure system or Aleutian Low in winter and the high pressure system or North Pacific High in summer. These two systems govern the distribution of mean surface winds over the Northeast Pacific Ocean. In winter the Aleutian Low directs air flow northward into the Gulf of Alaska, while in summer the North Pacific High directs winds southeast at Ocean Station "P." Additionally, monthly mean wind speeds are approximately twice as large in magnitude ( $13\text{m/s}$ ) in winter as in summer ( $6\text{m/s}$ ).

Station "P" is located in a distinct oceanic regime (Fig. 2 on page 7). The surface waters of the region are under the influence of the weak westward flow. Specifically, this flow is composed of the West Wind Drift and the recirculated waters from the Alaska Stream. The former carries mixed waters of the Kuroshio and the Oyashio, which are generally indistinguishable by the time that they reach Ocean Station "P." To the east of this area, the current turns north, forming the Alaskan current.

The vertical structure of this water is characterized by three zones: (1) the upper "seasonal" zone (0-100m), (2) the halocline (100-200m), and (3) the lower zone ( $> 200\text{m}$ ). Within the upper zone the salinity is relatively low ( $\sim 32.7\text{ppm}$ ). With respect to seasonal effects, in winter the temperature and salinity in zone 1 are relatively homogeneous and isothermal. In summer a significant vertical salinity gradient exists in this uppermost zone, as well as a well defined thermocline, with a temperature decrease with depth of as much as  $8^{\circ}\text{C}$  per 20m. In the halocline, zone 2, salinity increases with depth by as much as  $1.0\text{ppm}$  per 100m. In zone 2 temperature decreases with depth typically, unless an inversion is present. In the lower zone salinity increases only gradually with depth, while temperature decreases gradually with depth (Fig. 3 on page 8).

Tabata (1961) indicates that there is an annual average excess of precipitation over evaporation of  $\sim 0.5\text{m}$ . Garzon (1987) also estimates an excess annual precipitation. Despite this annual excess of precipitation, salinity within the water column does not decrease on an annual time scale, although it can vary as noted by Tabata (1961).

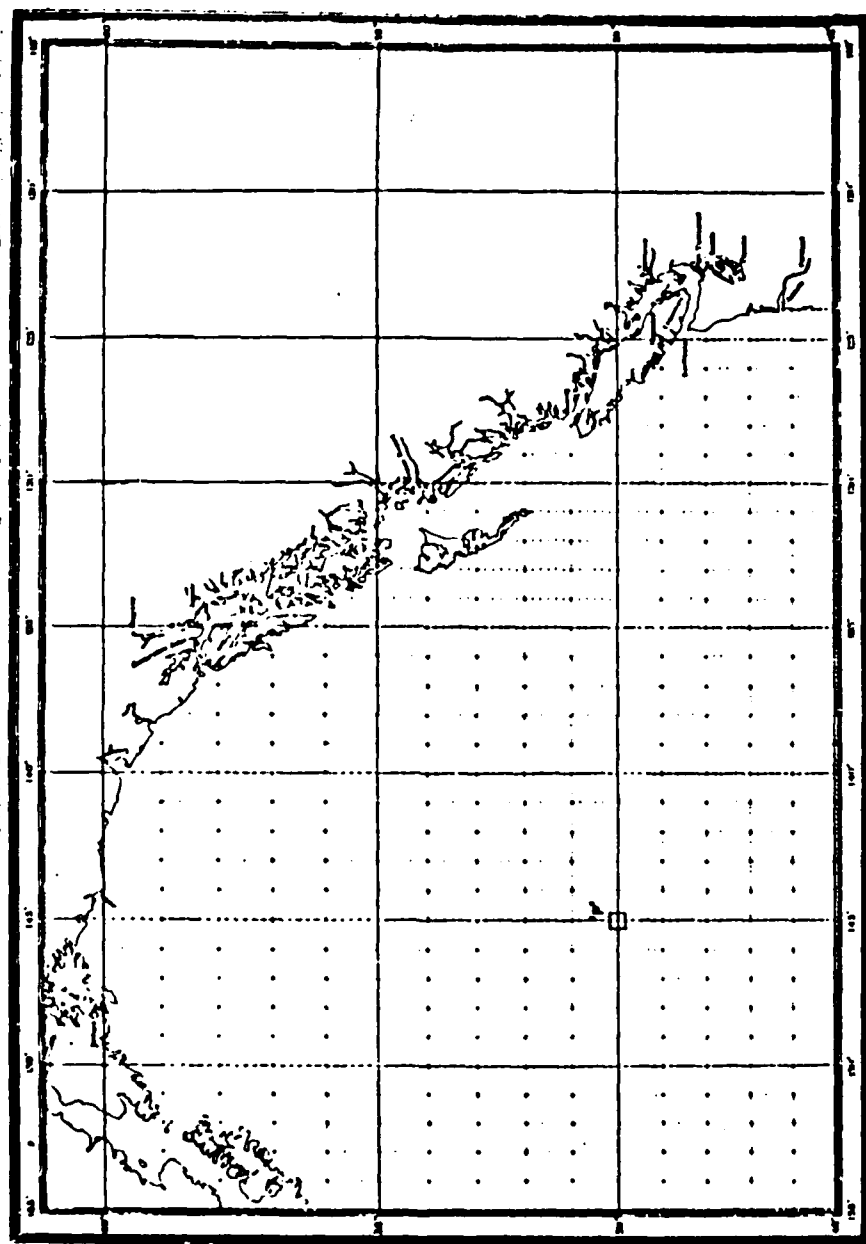


Fig. 1. Region Surrounding Ocean Station "P" (from Tabata, 1961)

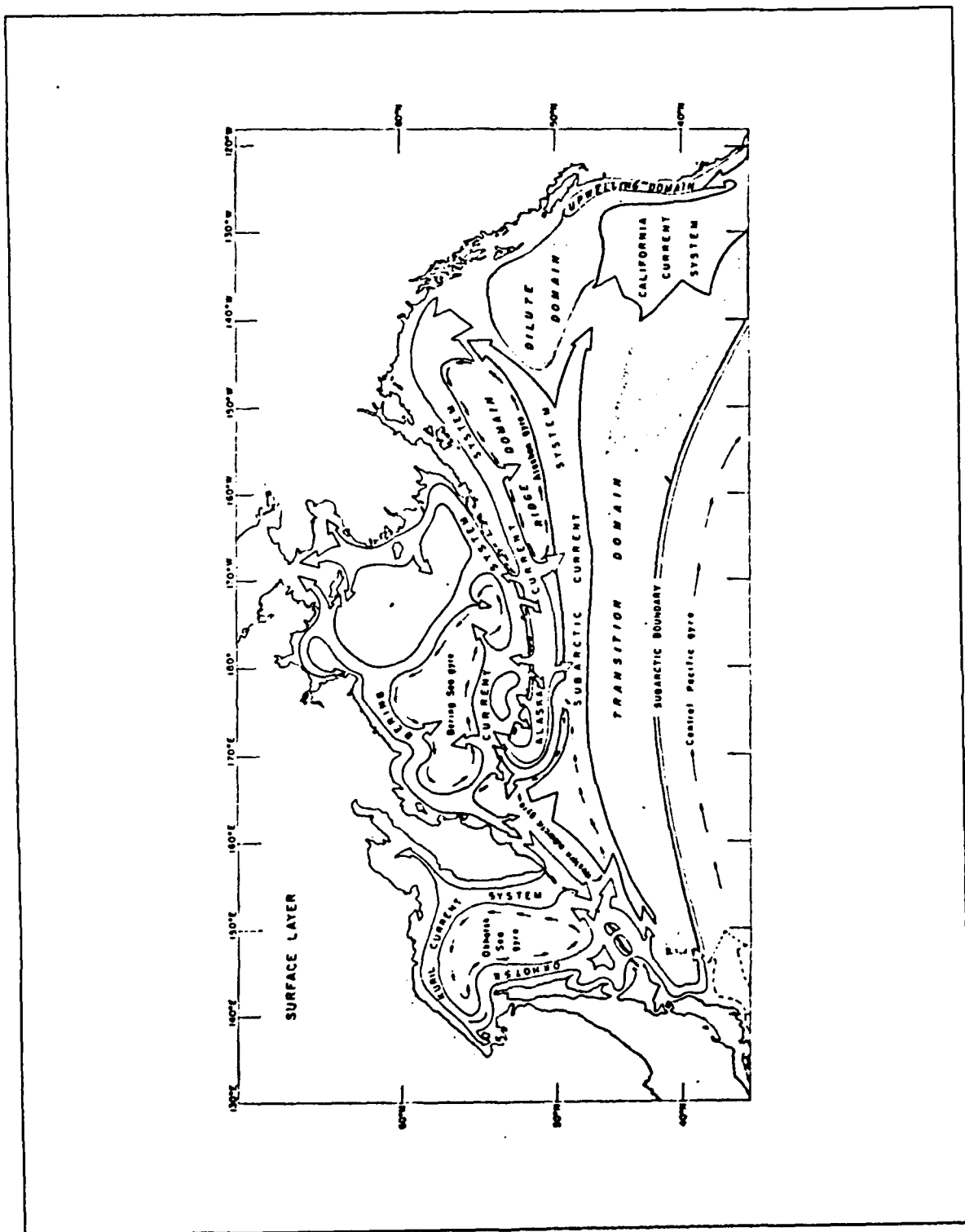


Fig. 2. Oceanic Regime at Station "P." (from Favorite, 1976)

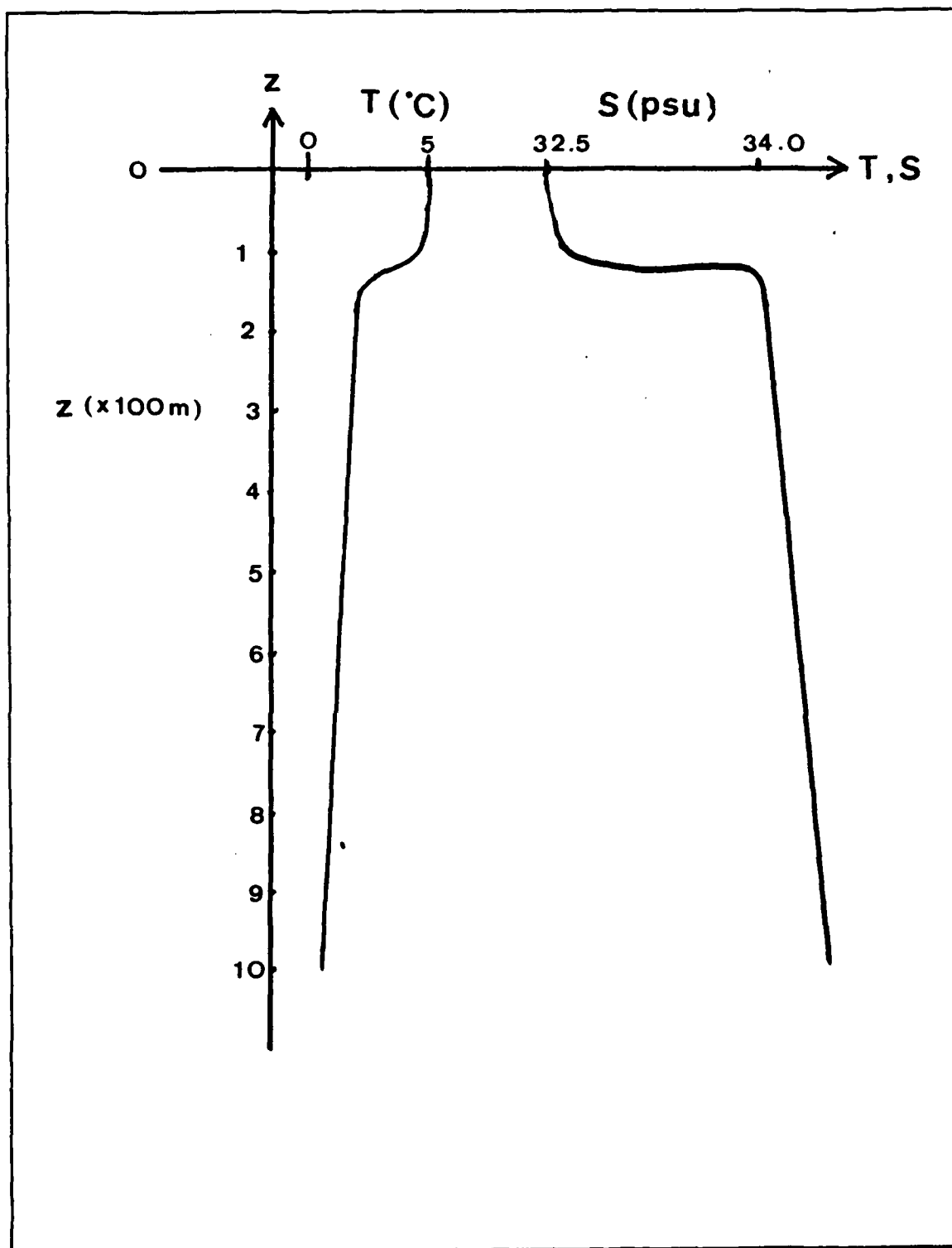


Fig. 3. Example Temperature and Salinity Profiles



especially within the more dynamic mixed layer. Horizontal advection must account for this readjustment. As noted by Tabata, upwelling is weak and nearly insignificant within these waters, when compared with horizontal advection. As a result this salinity balance appears to be maintained by horizontal advection as more saline water is transported into the area by ocean currents.

Despite the consistent westerly current coming into this area, anomalous events have occurred resulting in horizontal transport of water into the area from a non-westerly direction. Tabata (1961) noted an unusual increase in temperature and decrease in salinity within the upper zone and halocline during spring 1957 through summer 1958. This was attributed to transport in water lying south of Ocean Station "P" into the study area. The suggested cause for this transport was the shift of winds in the region associated with unusual location of the atmospheric pressure system over the northeast Pacific Ocean. This displacement of the North Pacific High yielded westerly instead of the usual southeasterly winds, which could have generated southerly drift currents in the vicinity of the station.

Overall, the currents in this area are weak. Except for occasional anomalous transport associated with unusual synoptic weather systems, salinity follows a roughly annual cycle maintained by horizontal advection, and the waters of the study area are relatively homogeneous horizontally. These factors combine to provide an excellent region for a one-dimensional modeling study of the thermodynamics of the upper ocean.

## II. DATA SOURCES AND PREPARATION

### A. DATA SOURCES

This study was performed using various sources. Atmospheric forcing data was originally obtained from the National Weather Records Center, Asheville, North Carolina. This data included three-hourly observations of wind direction and speed, air temperature, sea surface temperature, dew point temperature and cloud coverage in octaves. Atmospheric data was interpolated from three hourly to one hourly data for computation of hourly surface fluxes. Precipitation forcing data was not directly available and was derived as explained later in this chapter.

Two types of oceanic data were used. CTD/STD data was provided by the Marine Environmental Data Service, Ottawa, Canada. These salinity and temperature casts were digitized from depths of 0 to 1500 m at various intervals, with more concentrated data provided within the mixed layer. These casts were not taken at regular intervals, but were taken as operationally feasible. There were 119 casts available for analysis during the study period from station "P." Bathythermograph casts were not available for this time period.

Three hourly atmospheric forcing data was used in this study to compute the fluxes of heat, radiation and momentum necessary for forcing the mixed layer model with an hourly time step. Specifically, these boundary conditions were wind stress in two-dimensional components, incident solar radiation, heat loss (long and short wave), and precipitation and evaporation. The calculation of precipitation will be discussed later. Temperature and salinity profiles from STD taken 23 November 1969 were used to initialize the model profiles, and CTD/STD casts were used for verification. Bucket temperatures were used for comparison of with predicted temperature.

### B. VERTICAL INTERPOLATION

The oceanic profiles, from both CTD/STD sources were vertically interpolated from 0 to 199 m to a standard grid of 1 m spacing. Mixed layer depth, mixed layer temperature, and mixed layer salinity were derived from these interpolated profiles. There is not a standard way to compute mixed layer depth from a CTD/STD profile. For this study the mixed layer depth has been defined to be that depth at which the temperature profile changes exceed  $0.10^{\circ}\text{C}$  in 5 m. Mixed layer temperature and mixed layer salinity

values were obtained by averaging temperature from 1 m to the mixed layer depth as determined above.

### III. THEORY

#### A. OCEANIC MIXED LAYER STRUCTURE

A familiarization with the definitions associated with the oceanic mixed layer thermal structure is required to understand the dynamics involved in mixed layer modeling. As defined in Garzon (1987) the oceanic mixed boundary layer is assumed to be the fully turbulent region of the upper ocean bounded above by the air-sea interface and below by a relatively static water mass. The mixed layer is considered to be "quasi-homogeneous," that is, it is approximated to be well mixed. Thus temperature within the mixed layer is considered to be relatively constant. Fig. 4 on page 13 graphically depicts an oceanic vertical temperature profile. The turbulent mixed layer of depth  $h$  is contained within the upper most oceanic region, below which lies the turbulent entrainment zone, from depths  $z = -h$  to  $z = -h - \delta$ , with  $z$  positive upward. Within the entrainment zone there is a temperature jump of  $\Delta T$ . Below the entrainment zone is the quasi-stable water mass and here temperature decreases with increasing depth.

Mixed layer structure (Fig. 5 on page 14) for salinity is similar to that for temperature (Fig. 4 on page 13). There is a relatively constant salinity within the turbulent mixed layer from  $z = 0$  to  $z = -h$ , a salinity jump  $\Delta S$  across the entrainment zone from  $z = -h$  to  $z = -h - \delta$ , and a gradually increasing salinity with depth below the mixed layer.

An oceanic mixed layer prediction scheme requires an accurate (or near accurate) assessment of the deepening or shallowing rate of that layer. Garwood (1977) accounted for both of these processes. The equations used by Garwood to best describe these processes are developed as follows.

#### B. ENTRAINMENT

The Garwood (1977) one-dimensional mixed layer model considers both turbulent erosion and dynamic instability. Fundamental to the solution of this model is an accurate assessment of the entrainment velocity,  $W_e$ . Starting with:

$$\frac{\partial h}{\partial t} = W_e - W(-h) \quad (3.1)$$

Assuming no mean vertical motion,  $W(-h) = 0$ , this equation becomes:

$$W_e = \frac{\partial h}{\partial t} \quad (3.2)$$

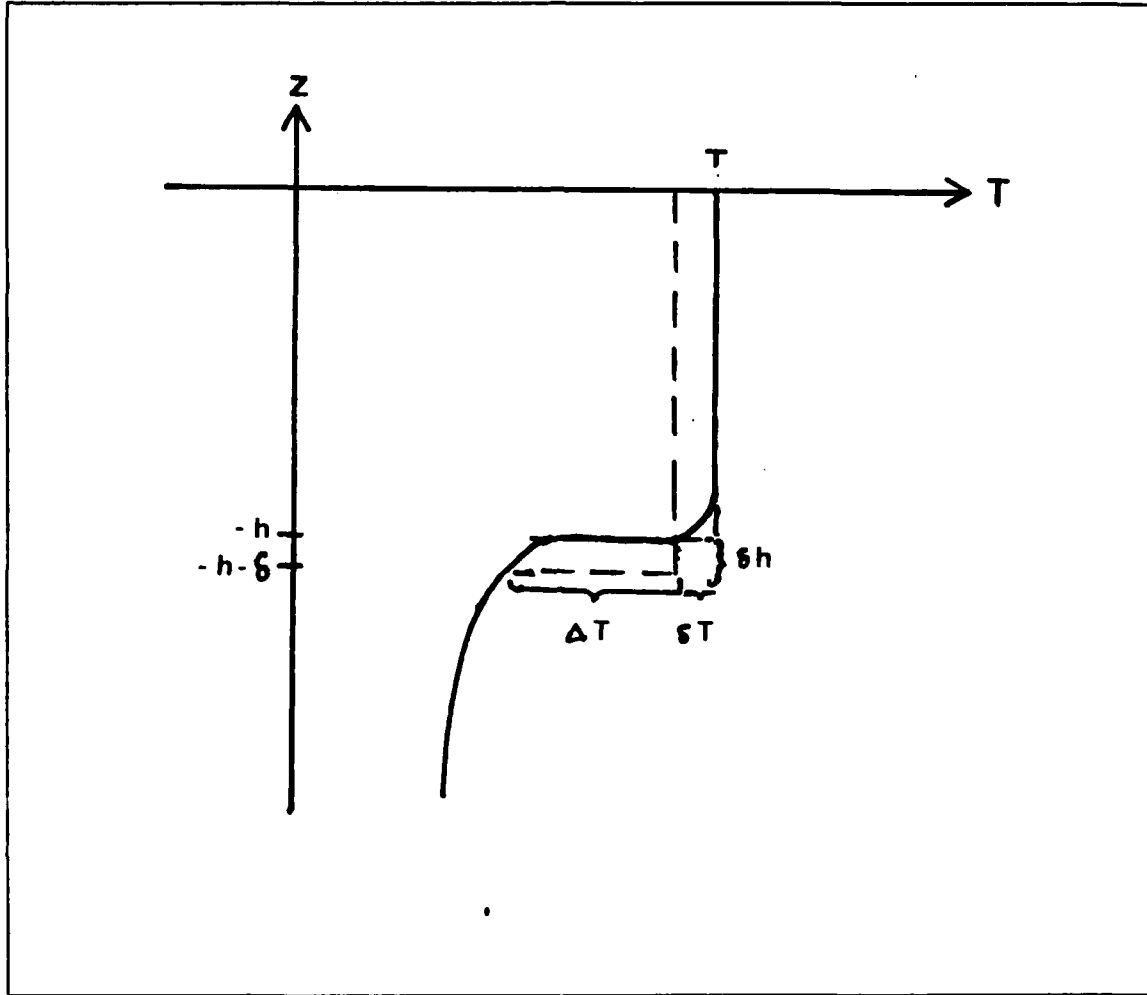


Fig. 4. Example Temperature Profile

The solution for  $W_z$  can be found by solving the total turbulent kinetic energy (TKE) budget written as:

$$\frac{\partial}{\partial t} \frac{\bar{E}}{2} = \left[ -\overline{U'W'} \frac{\partial \bar{U}}{\partial z} - \overline{V'W'} \frac{\partial \bar{U}}{\partial z} \right] + [\alpha g \overline{T'W'}] - \frac{\partial}{\partial t} \left[ \overline{W' \left( \frac{E}{2} \frac{P'}{\rho_0} \right)} \right] - \epsilon \quad (3.3)$$

where:

$\bar{E} = \overline{U'^2} + \overline{V'^2} + \overline{W'^2}$ , is the Total TKE.

(see Table 1 on page 20 for definitions of constants)

The five terms in Equation (3.3) from left to right are:

1. the time rate of change of turbulent kinetic energy,

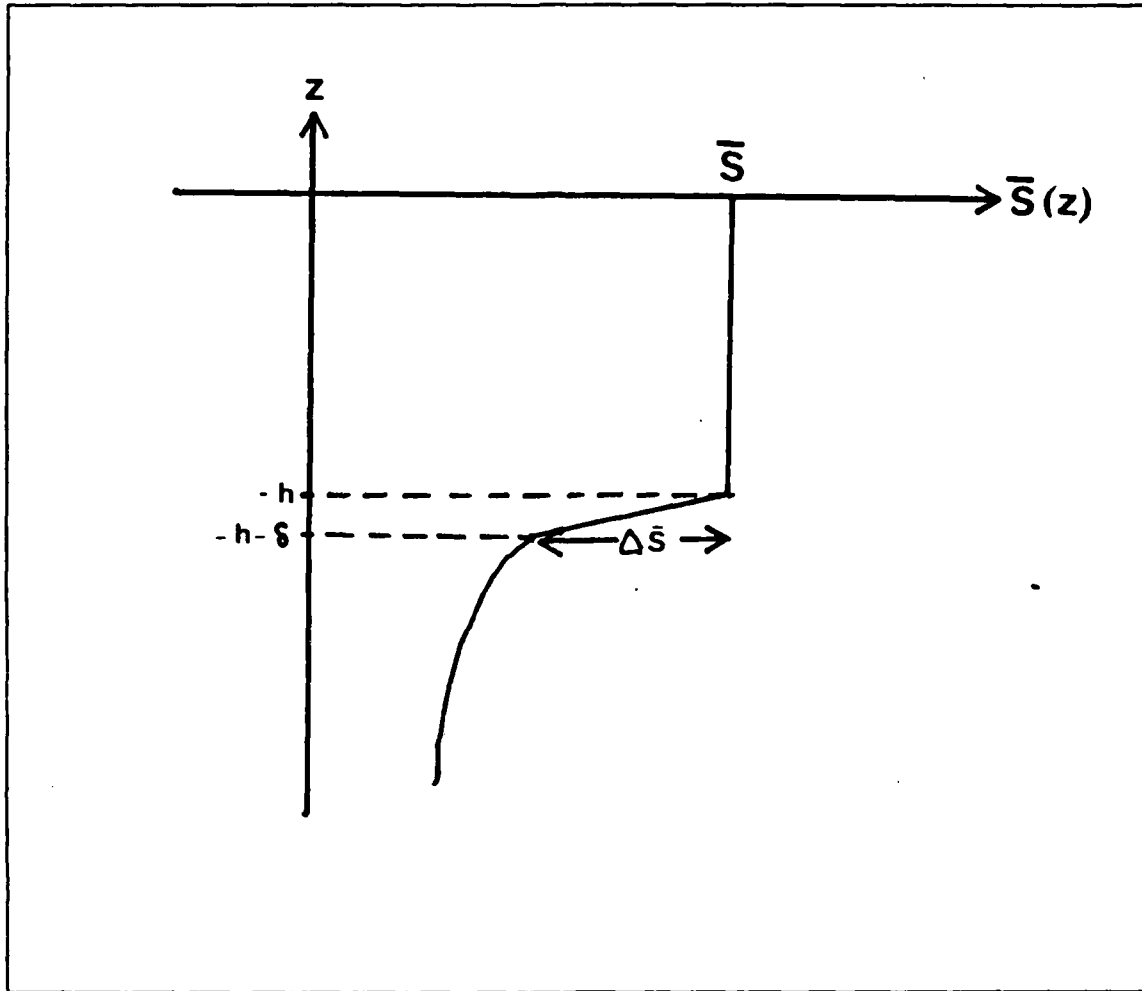


Fig. 5. Example Salinity Profile

2. shear production,
3. buoyancy flux,
4. turbulent diffusion (or redistribution), and
5. viscous dissipation.

This equation may be examined for the entrainment zone. Within the entrainment zone, dissipation and shear production are assumed negligible. This produces a mean turbulent kinetic energy equation for the entrainment zone of the form

$$\frac{\partial}{\partial t} \frac{\bar{E}}{2} = \alpha g \overline{T'W'} - \frac{\partial}{\partial z} \overline{W' \left( \frac{E}{2} + \frac{P'}{\rho_0} \right)} \quad (3.4)$$

across the entrainment zone of thickness  $\delta$ . Integrating equation (3.4) yields:

$$\int_{-h-\delta}^{-h} \frac{\partial}{\partial t} \frac{\bar{E}}{2} dz = \int_{-h-\delta}^{-h} \alpha g \overline{T W'} dz - \left[ \overline{W' \left( \frac{E}{2} + \frac{P'}{\rho_0} \right)} \right]_{-h-\delta}^{-h} \quad (3.5)$$

Assuming steady state, the time rate of change of turbulent energy may be neglected. Equation (3.5) becomes:

$$\int_{-h-\delta}^{-h} \alpha g \overline{T W'} dz - \left[ \overline{W' \left( \frac{E}{2} + \frac{P'}{\rho_0} \right)} \right]_{-h-\delta}^{-h} = 0 \quad (3.6)$$

Solving this integral produces equation (3.7).

$$\frac{\alpha g \delta}{2} (\overline{T W'}|_{-h} + \overline{T W'}|_{-h-\delta}) - \overline{W' \left( \frac{E}{2} + \frac{P'}{\rho_0} \right)}|_{-h-\delta} = 0 \quad (3.7)$$

When specifically examining this equation at the base of the mixed layer (or the top of the entrainment zone):

$$\alpha g \overline{T W'}|_{-h} = \frac{\partial}{\partial z} \overline{W' \left( \frac{E}{2} + \frac{P'}{\rho_0} \right)}|_{-h} \quad (3.8)$$

Kraus and Turner simplified the solution at this point by neglecting the redistribution term and combining the entrainment mean kinetic energy equation with the steady state turbulent kinetic energy equation for the mixed layer. Garwood does not neglect this term, but estimates its magnitude with the following parameterization:

$$-\frac{\partial}{\partial z} \overline{W' \left( \frac{E}{2} + \frac{P'}{\rho_0} \right)}|_{-h} = \frac{\langle \bar{E} \rangle}{\tau_e} \quad (3.9)$$

Thus the redistribution term is equal to the mean turbulent energy available near the base of the mixed layer divided by the time scale required to transport this energy into the area. Parameterizing this time scale as

$$\tau_e \sim \frac{h}{|W'|}, \quad (3.10)$$

where  $|W'|$  is the root-mean square vertical turbulent velocity,  $|W'| = (\overline{W'^2})^{1/2}$ , and the time scale is approximated as the absolute value of the mixed layer depth divided by the absolute value of the vertical velocity.

Using Equations (3.8 to 3.10) and assuming that  $\overline{T'W'}|_{-h} = \Delta T W_e$ ,

$$g(\alpha\Delta T - \beta\Delta S)W_e = \frac{\langle \bar{E} \rangle |W''|}{h} \quad (3.11)$$

Here vertical transport of turbulence exactly balances entrainment buoyancy flux. This equation may be solved for the entrainment velocity:

$$W_e = \frac{|W''| \langle \bar{E} \rangle}{hg(\alpha\Delta T - \beta\Delta S)} \quad (3.12)$$

To solve this equation for  $W_e$ , the values of  $\langle \bar{E} \rangle$ ,  $|W''|$ ,  $T$ ,  $h$ , and  $\Delta T$  must be known while  $g$  and  $\alpha$  are constants (Table 1 on page 20). From Garwood (1977) the total turbulent kinetic energy is solved by using:

$$\frac{\partial}{\partial t} (h \langle \bar{E} \rangle) = G_0 + G_h - B_0 - B_h - D \quad (3.13)$$

In order to solve equation (3.13), the following equations for shear production at  $z=0$  and  $z=-h$ , and buoyancy damping production at  $z=0$  and  $z=-h$ , and dissipation are:

wind shear production,

$$G_0 = 12 \left[ \left( \frac{\tau_x}{\rho} \right)^2 + \left( \frac{\tau_y}{\rho} \right)^2 \right]^{3/4}, \quad (3.14)$$

entrainment shear production,

$$G_h = [ \langle \bar{u} \rangle^2 + \langle \bar{v} \rangle^2 ] W_e, \quad (3.15)$$

where the x and y components of the mixed layer current are:

1.  $\frac{\partial}{\partial t} (h \langle \bar{u} \rangle) = fh \langle v \rangle + \frac{\tau_x}{\rho}$ , and
2.  $\frac{\partial}{\partial t} (h \langle \bar{v} \rangle) = fh \langle u \rangle + \frac{\tau_y}{\rho}$ .



buoyant damping production due to surface buoyancy,

$$B_0 = \alpha g \left[ \frac{Q_0}{\rho C_p} \right] - \beta g \bar{S}(E - P), \quad (3.16)$$

buoyant damping due to entrainment,

$$B_h = \alpha g h \Delta \bar{T} W_e, \text{ and} \quad (3.17)$$

dissipation,

$$D = 2 < \bar{E} >^{3/2}. \quad (3.18)$$

### C. MIXED LAYER THERMODYNAMICS: TEMPERATURE AND SALINITY BUDGETS

Wind stress generated turbulence at the air-sea interface provides the energy to destabilize and entrain the water below. This mixing process deepens the mixed layer and mixes temperature and salinity between the surface and the entrainment zone. Thus, the conservation of heat requires that:

$$\frac{\partial \bar{T}}{\partial t} = - \frac{\partial \overline{T'W'}}{\partial z} \quad (3.19)$$

Vertically integrating Equation (3.19) across the entrainment zone,  $z = -h - \delta$  to  $z = -h$ , and assuming  $\overline{T'W'}$  vanishes below  $z = -h - \delta$  gives

$$- \Delta \bar{T} W_e = \overline{T'W'}(-h) \quad (3.20)$$

where:

$$\Delta \bar{T} = \bar{T}(z = -h) - \bar{T}(z = -h - \delta).$$

Vertically integrating Equation (3.19) across the entire mixed layer,  $z = -h$  to  $z = 0$  gives

$$\int_{-h}^0 \frac{\partial \bar{T}}{\partial t} dz = \int_{-h-\delta}^0 - \frac{\partial \overline{T'W'}}{\partial z} dz \quad (3.21)$$

Using Equation (3.20) and assuming  $\bar{T}$  to be well mixed in  $z$ , Equation (3.21) becomes

$$\frac{\partial T}{\partial t} = \frac{\overline{T W'}(0)}{h} + \frac{\overline{T W'}(-h)}{h} \quad (3.22)$$

or

$$\frac{\partial T}{\partial t} = \frac{Q_0}{\rho C_p h} - \frac{\Delta \bar{T} W_e}{h} \quad (3.23)$$

Here :

1.  $\Delta \bar{T} = \bar{T} - \bar{T}(-h - \delta)$ , and
2.  $Q_0 / \rho C_p = -\overline{T W'}(0)$ .

The one-dimensional salinity budget for the oceanic mixed layer is:

$$\frac{\partial S}{\partial t} = - \frac{\partial \overline{W' S'}}{\partial z} \quad (3.24)$$

It is assumed that:

1.  $S(z)$  is well mixed from the bottom of the mixed layer to the top of the mixed layer,
2.  $S(z)$  has a near discontinuity between  $z = -h$  and  $z = -h - \delta$ , and
3. the vertical flux of  $S$  (or  $\overline{S' W''}$ ) vanishes at  $z \leq -h - \delta$ .

Fig. 5 on page 14 depicts this condition. Here the turbulent region within the mixed layer yields a near homogeneous state with respect to salinity. Examining Equation (3.24) and integrating gives:

$$\int_{-h(t)-\delta}^{-h(t)} \frac{\partial \bar{S}}{\partial t} dz = \int_{-h-\delta}^{-h} \frac{\partial \overline{W' S'}}{\partial z} dz \quad (3.25)$$

With  $h$  variable in time, application of the Leibnitz Rule of integration and assuming  $\delta$  is vanishing small,

$$\Delta \bar{S} \frac{\partial h}{\partial t} = -\overline{W' S'}(-h) + \overline{W' S'}(-h - \delta). \quad (3.26)$$

Assuming that turbulence is negligible below the mixed layer, i.e.  $\overline{W' S'}(-h - \delta) \sim 0$ . This makes the "jump condition" for salinity entrainment into the mixed layer:

$$\Delta \bar{S} \frac{\partial h}{\partial t} = -\overline{W' S'}(-h). \quad (3.27)$$

where:

$$\Delta \bar{S} = \bar{S}(z = -h) - \bar{S}(z = -h - \delta)$$

#### D. SALINITY EFFECT ON MIXED LAYER DYNAMICS

##### 1. The Shallowing Effect

Kraus and Turner's (1967) model provides an approximation for the non-entraining or shallowing mixed layer,  $W_e = 0$ ,

$$h = \frac{C_1}{C_2} \frac{U_*^3}{\alpha g Q_0 / (\rho C_p)} = L. \quad (3.28)$$

Here  $L$  is the Obokov length scale and equation (3.28) is the solution when there is no entrainment. The surface buoyancy flux is  $B_0 = (\alpha g q_0 / (\rho C_p))$  and  $U_*$  is the surface friction velocity, with  $U_*^2 = (\rho_s / \rho) C_D \bar{U}^2$ . The value of  $h$  is inversely proportional to  $Q_0$ . The mixed layer temperature is even more sensitive to  $Q_0$  than is  $h$ :

$$\frac{\partial T}{\partial t} = Q_0 / (\rho C_p h) \propto Q^2 \propto \frac{1}{h^2} \quad (3.29)$$

If the buoyancy flux attributable to precipitation and evaporation is included, Equation (3.28) becomes

$$h = \frac{C_1}{C_2} \frac{U_*^3}{\alpha g Q_0 / (\rho C_p) + \beta g (P - E) S}. \quad (3.30)$$

Where the salinity concentration coefficient,  $\beta = 0.76 \times 10^{-3} \text{ Kg/gm}$ , and  $P-E$  is the net precipitation minus evaporation in m sec. With the salinity flux included, the surface buoyancy flux becomes:

$$B_0 = \alpha g Q_0 / \rho C_p + \beta g (P - E) S, \quad (3.31)$$

and the effect on mixed layer temperature becomes:

$$\frac{\partial T}{\partial t} = (Q_0 / \rho C_p) / h \alpha Q_0 (Q_0 + \beta / \alpha (P - E) S). \quad (3.32)$$

As a result, precipitation minus evaporation influences mixed layer temperature indirectly. For positive  $Q_0$  (net heat into the surface), a positive  $(P-E)$  will decrease  $h$ , concentrating the heat into a shallow layer. For the case where evaporation exceeds precipitation a decrease of mixed layer temperature with respect to time results.

## 2. The Deepening Effect

For entraining, deepening mixed layers, the buoyancy discontinuity at the bottom of the mixed layer must be augmented to include a possible salinity jump:

$$\Delta b = \alpha g \Delta T - \beta g \Delta S \quad (3.33)$$

where:

$$\Delta \bar{S} = \bar{S} - \bar{S}(-h - \delta),$$

$\bar{S}$  is the mixed layer salinity, and

$\bar{S}(-h - \delta)$  is the salinity just below the mixed layer.

The mixed layer salinity budget is:

$$\frac{\partial \bar{S}}{\partial t} = \frac{S(E - P)}{h} - \frac{W_e \Delta \bar{S}}{h} \quad (3.34)$$

Equation (3.34) demonstrates that the change in salinity with respect to time depends on fresh water flux at the surface, entrainment velocity, salinity advection, mixed layer depth, and upon the salinity jump at the base of the mixed layer.

Table 1. MODEL CONSTANTS

Model Constants		
constant	definition	value
$\alpha$	thermal expansion coefficient	$\sim 10^{-3} K^{-1}$
$\beta$	salinity expansion coefficient	$\sim 8 \times 10^{-4} ppm^{-1}$
$C_1$	tuning coefficient	$\sim 1$
$C_2$	tuning coefficient	$\sim .2$
$C_p$	specific heat	$\sim 4000 J \cdot kg^{-1} \cdot K^{-1}$
$\rho$	sea water density	$\sim 1026.5 kg \cdot m^{-3}$

## IV. HYPOTHETICAL EXPERIMENTS

### A. EFFECTS OF DISCRETE PRECIPITATION EVENTS

The purpose of this study was to determine the lasting effects of discrete precipitation events on the mixed layer. For "case 1" in this study short-term precipitation events of 10 cm in one day with no evaporation was applied monthly to the Garwood (1977) model over a 365 day study period. This yielded twelve separate events for detailed study. At all other times during the year both evaporation and precipitation were assumed to zero. The resulting output from the model was examined individually for 30 day periods following each rain event to better reveal long term trends. The precipitation event was applied on the fourth day of each monthly period. Actual temperature and salinity profiles taken from a CTD cast for November 23, 1968 were used as initial conditions. Heat and momentum fluxes were computed from the actual surface meteorological and observations.

Fig. 6 on page 22 and Fig. 7 on page 23 are a conglomeration of the results of these twelve separate events. Other figures in this chapter represent the individual events that were selected for closer examination at a 60 day period.

The effects of precipitation events on the MLD are graphically represented by the figures in this chapter. The equations developed in Chapter 3 will be used to explain the results and are repeated here:

$$\frac{\partial T}{\partial t} = \frac{Q_0}{\rho C_p h} - \frac{\Delta T W_e}{h} \quad (4.1)$$

The change in mixed layer temperature (T) with respect to time is a function of:

1. MLD,  $h$ ,
2. entrainment rate,  $W_e$ ,
3. temperature jump at the base of the mixed layer,  $\Delta T$ , and
4. net downward heat flux,  $Q_0$ .

For a case of no entrainment,  $W_e = 0$ , the temperature will rise for  $Q_0 > 0$ , and it will fall for  $Q_0 < 0$ . The rate of rise and fall is inversely proportional to  $h$ . If  $Q_0 \leq 0$  and there is entrainment,  $W_e > 0$ , the mixed layer temperature can only decrease if  $\Delta T > 0$ . The

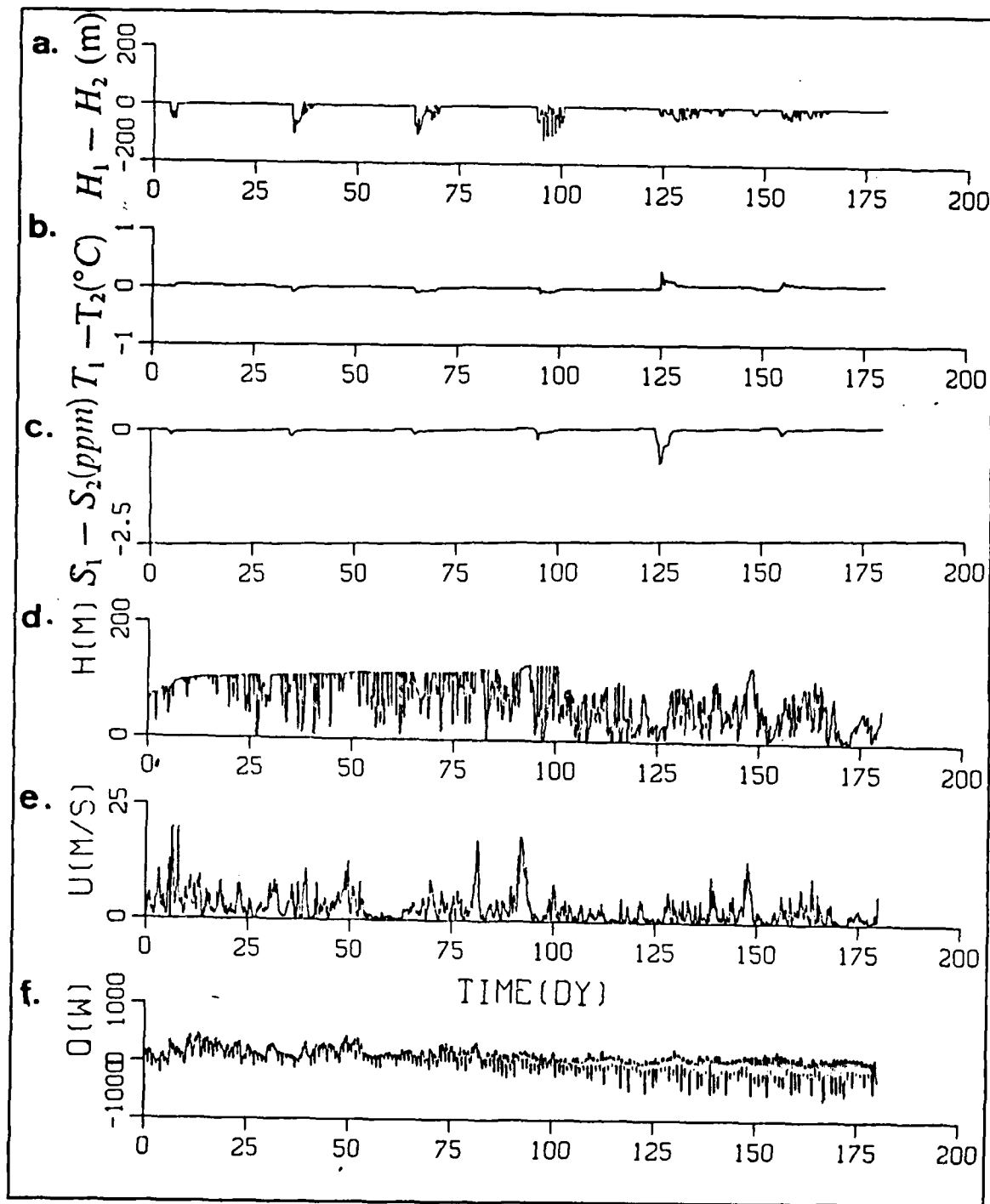


**Fig. 6.** Conglomeration of Six Events (Dec 1968 to May 1969): (a) differential MLD, (b) differential temperature, (c) differential salinity, (d) MLD with  $E-P=0$ , (e) wind speed, and (f) net surface heat flux.

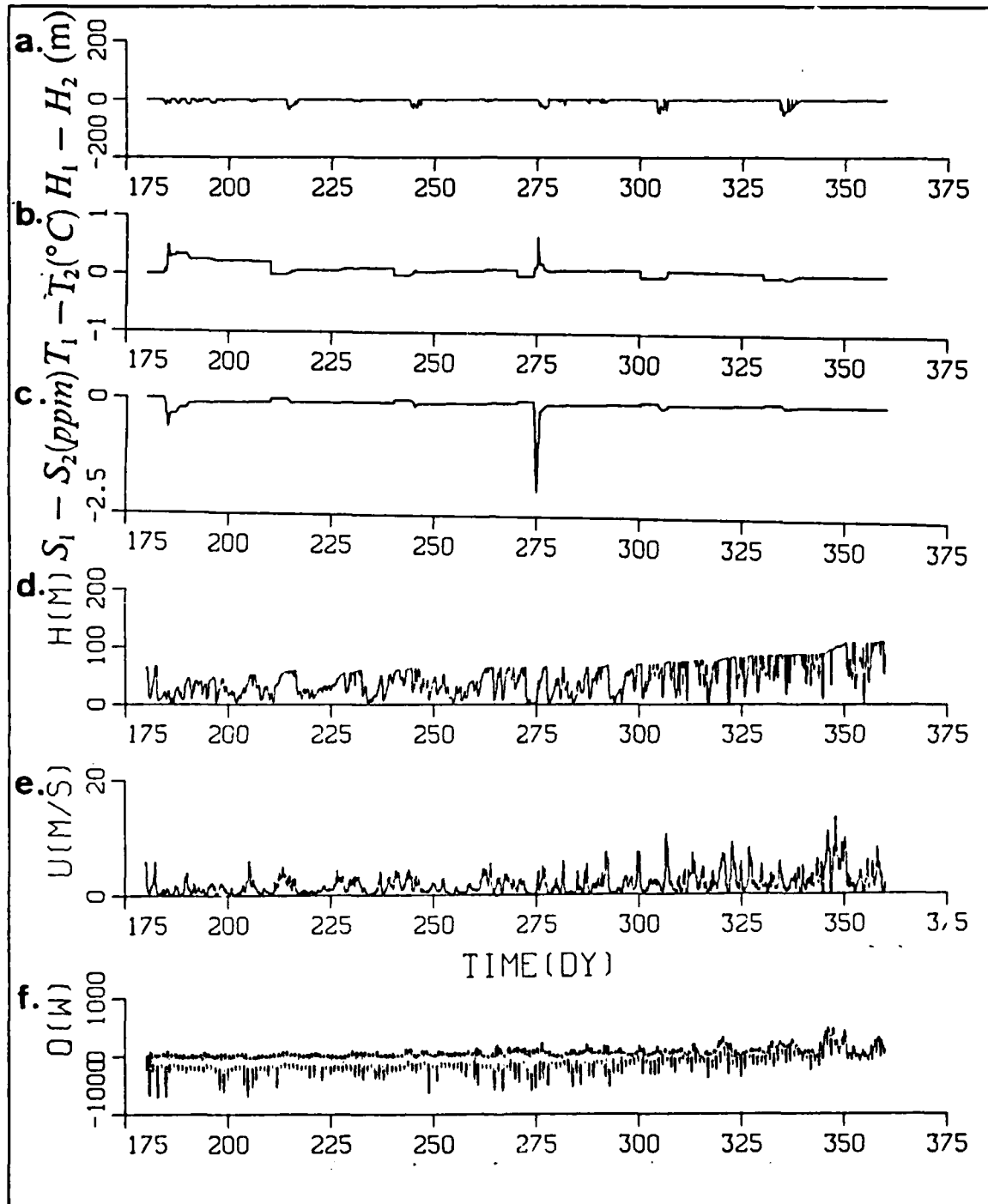


Fig. 7. Conglomeration of Six Events (Jun to Nov 1969): (a) differential MLD, (b) differential temperature, (c) differential salinity, (d) MLD with  $E-P=0$ , (e) wind speed, and (f) net surface heat flux.

rate of decrease is greatest for small  $h$ . Various factors effect  $W_e$ , and will be considered later.

Two model predictions may be compared. In this experiment the first case included the discrete precipitation event, while the second case had no events, with  $E-P=0$  for the entire model integration. When subtracting the results of one study using equation (4.1) from another such study for the same time using the same equation, the results provide:

1. differential MLD ( $h_1 - h_2$ ),
2. differential temperature ( $T_1 - T_2$ ), and
3. differential salinity ( $S_1 - S_2$ ).

Differentiating the differential temperature with respect to time yields:

$$\frac{\partial(T_1 - T_2)}{\partial t} = \left( \frac{1}{h_1} - \frac{1}{h_2} \right) \frac{Q_0}{\rho C_p} - \left[ \frac{\Delta T_1 W_{e1}}{h_1} - \frac{\Delta T_2 W_{e2}}{h_2} \right] \quad (4.2)$$

Therefore, in order to provide a value other than zero for  $\partial(T_1 - T_2)/\partial t$ , the differential temperature, one or more of the following conditions must exist:

1.  $h_1 \neq h_2$ ,
2.  $W_{e1} \neq W_{e2}$ , and
3.  $\Delta T_1 \neq \Delta T_2$ .

Again, considering the many variables that may alter the entrainment rate, there are numerous factors which may effect this differential temperature, making interpretation of even a simple precipitation event complex, but more easily examined than the case with a more realistic and complex E-P time series of forcing.

Initially, in all twelve events with all forcing values equal (for the first five days), the differential temperature  $\delta T = T_1 - T_2$  must equal zero. This can be seen in Fig. 6 on page 22 and Fig. 7 on page 23 for the first five days of each 30-day period. Upon initiation of the precipitation event at day five of each events  $h_1 = h_2$  and  $\Delta T_1 = \Delta T_2$ , but  $W_e$  is instantaneously altered in the precipitation case. In this case with  $E-P < 0$ , there results in an immediate increase of surface buoyancy,  $B_0$ ,

$$B_0 = \alpha g \left[ \frac{Q_0}{\rho C_p} \right] - \beta g \bar{S} (E - P).$$

An increase in  $B_0$  acts to decrease the total TKE from equation (3.13),



$$\frac{\partial}{\partial t} (h < E >) = G_0 + G_h - B_0 - B_h - D$$

and, therefore, entrainment rate from equation (3.12),

$$W_e = \frac{|W'| < \bar{E} >}{gh(\alpha\Delta T - \beta\Delta S)}.$$

As  $W_e$  decreases, so will MLD, which acts dynamically to shallow the MLD relative to the case with  $P-E=0$ . Thus a precipitation event increases the downward surface buoyancy through decreasing salinity, which ultimately results in a shallower MLD. This initial result should be apparent throughout the twelve experiments where there is precipitation.

While the immediate change in MLD through reduced entrainment is expected on a short time scale (during the rain event), longer term changes in mixed layer dynamics may result from a single short-term precipitation event. In response to mixed layer shallowing, MLD and the temperature jump at the base of the mixed layer will change from that of the non-precipitation case. At this point all three possible conditions required to yield an increase in the differential temperature may exist.

Thus analysis of the effects of a discrete precipitation event requires a case by case examination. Any differences in MLD will yield a non-zero magnitude of  $|h_1 - h_2|$  which will effect the differential temperature. A fluctuation in differential MLD will also moderate the effects of  $Q_0$ ,  $\Delta T_1 - \Delta T_2$ , and  $W_{e1} - W_{e2}$ . Any difference in the temperature jumps,  $|\Delta T_1 - \Delta T_2| \neq 0$ , will also yield an associated change in the differential temperature and a transient response, as well as the altered value of  $W_e$ .

## B. ANALYSIS OF PRECIPITATION EVENT EFFECTS

### 1. Event #1 (Dec 1968)

Fig. 6 on page 22 represents the MLD output for the model with  $E-P=0$ . This figure indicates that this event began in the late-fall season when the mixed layer was at 80 m and deepening. Fig. 6 on page 22 and Fig. 8 on page 26 indicates that there was a net heat loss ( $Q_0 < 0$ ) during this period associated with a mid-latitude, winter regime. There were moderate winds during this time period ( $\bar{U} = 5.0m/s$ ), and maximum values of  $\bar{U}_{max} = 20.0m/s$  which occurred immediately before, during and after initiation of the precipitation event of day 5.

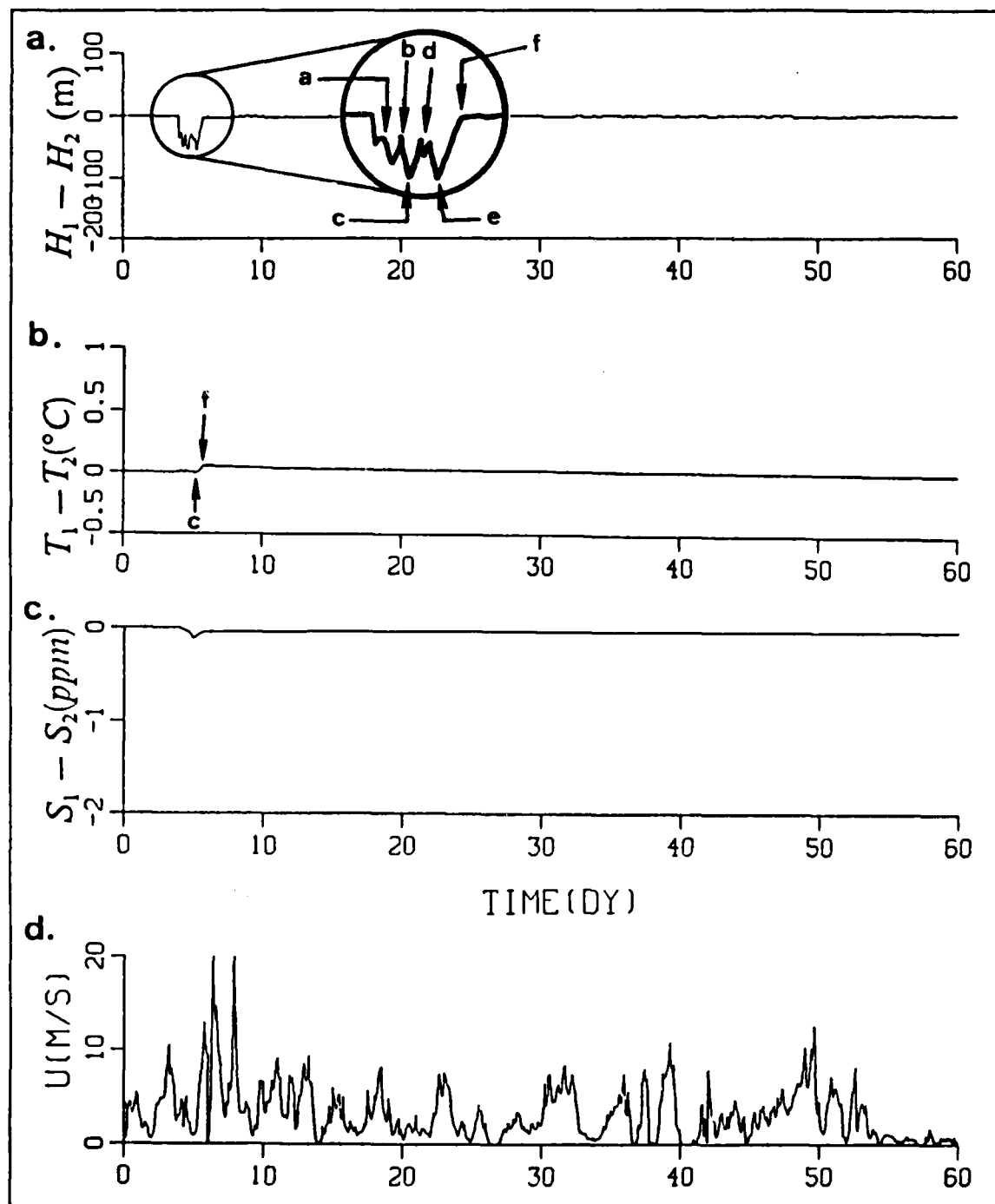


Fig. 8. Event #1 (Dec 1968): (a) differential MLD magnified from day 2 to day 8, (b) differential temperature, (c) differential salinity, and (d) wind speed

Prior to initiation of the precipitation event all differential values equaled zero (Fig. 6 on page 22 and Fig. 7 on page 23). This was true for all twelve events. Upon onset of precipitation at day four, MLD decreased from 65m to 10m, yielding a decrease in the differential MLD. This was coincident with shallowing of the mixed layer associated with a lull in wind. Approximately 12 hours after precipitation onset, however a moderate wind event followed immediately by another of magnitude  $U \sim 5.0\text{m/s}$  occurred. These increases in wind stress occurred during the precipitation event and resulted in two increases of the differential MLD and temperature (points a and b). Thus, the layer deepened, due to decreased  $W_e$ , causing the layer to cool.

Immediately following events a and b the wind decreased to near zero causing a large decrease in MLD. Here the differential MLD reached a maximum, as the MLD in case 1 shallowed to near the surface. Associated with this decrease in MLD in case 1, was a negative differential temperature. This was the result of the shallower MLD in case 1 allowing for the increased heat loss by the layer with  $Q_0 > 0$  (net heat loss) in winter (point c). The differential MLD increased then decreased, as induced by the onset and drop-off of a wind event (points d and e). Again this produced an associated positive and negative differential temperature, respectively. At day six a strong storm occurred, ( $U \sim 13.0\text{m/s}$ ) (event f) followed immediately by a series of larger fluctuations in wind speed. These storms brought the MLD of case 1 to near that of case 2. Increased buoyancy, causing decreased entrainment, caused the MLD in case 1 to deepen less than that of case 2 accounting for this significant differential temperature event at day six as case 1. This entrained less cold water than in case 2. After day six a series of winds ( $\bar{U} \sim 5.0\text{m/s}$ ) continued to mix the layer, bringing the differential MLD's and temperatures closer to zero. Although the effect of the precipitation event on the mixed layer decreased with time, the layer temperature and depth were effected measurably for this experiment period of 60 days.

There was an immediate decrease in salinity as precipitation diluted the layer, and this decrease continued until cessation of the precipitation event. Mixing by entrainment decreased the differential salinity to a value of -0.4ppm, after which time it rapidly approached that of case 2, aided by wind mixing.

## 2. Event #2 (Jan 1969)

As in Dec 1968, prior to the precipitation event the MLD was relatively deep ( $\bar{h} \sim 90\text{m}$ ) and continued to deepen during this winter regime. The values for  $Q_0$  still

indicated a net loss to the atmosphere and strong winds were predominate ( $\bar{U} \sim 5.0m/s$ ).

After the onset of the precipitation event, the results of the event were very similar to those of event #1. Therefore, no specific figures were provided other than those found between days 30 and 60 in Fig. 6 on page 22.

At the beginning of the precipitation, differential MLD generated a large decrease ( $\sim -100.0m$ ) as the MLD of case 1 nearly reached the ocean surface. This was concurrent with a wind speed lull for two days, enhancing this MLD shallowing. Associated with this MLD decrease was a decrease in the differential temperature as the shallower MLD in case 1 enhanced the temperature decrease associated with a net loss of heat in winter,  $Q_0 < 0$ . By day 40 a series of strong wind events ( $\bar{U} \sim 7.5m/s$ ) acted to converge the MLD of case 1 back to near that of case 2. Likewise, the differential temperature approached zero in a stepwise fashion as the temperature in case 1 approached that of case 2. Decreased entrainment rate due to increased buoyancy did not allow the MLD of case 1 to remain as deep as that of case 2. This caused the temperature of case 1 at day 33 to exceed that of case 2. It did not, however, exceed the increase seen in Event #1 as the difference in the MLD's between case 1 and case 2 were smaller in this event.

There was an immediate decrease in salinity as precipitation diluted the layer and this decrease continued until the end of the rain event. Mixing by diffusion and advection decreased the differential salinity to a value of -0.3ppm, after which time it rapidly approached that of case 2.

### 3. Event #3 (Feb 1969)

The MLD prior to the precipitation event was deep ( $\bar{h} \sim 95m$ ) and deepening during the winter regime. The value of  $Q_0$  still indicated a net loss of heat to the atmosphere, but the magnitudes of  $Q_0$  and of the wind speeds were smaller than for the previous two events.

After onset of the precipitation event in case 1, the results of the event were very similar to those of Event #1 and #2. As in Event #2, no specific figures were provided other than those found between days 60 and 90 in Fig. 6 on page 22. As the rain began, differential MLD generated a large negative event ( $\sim -70.0m$ ) as the MLD in case 1 nearly shallowed to the ocean surface. This was concurrent with a wind lull of four days, enhancing this shallowing. Associated with this MLD decrease was a decrease in the differential temperature as the shallower MLD in case 1 increased the temperature drop

associated with a net surface heat loss. During the end of the precipitation event there was a small peak in both the differential MLD's and temperatures associated with a wind speed maximum. By day 70 a series of strong wind events ( $\bar{U} \sim 5.0\text{m/s}$ ) caused the MLD of case 1 to converge to near that of case 2. Likewise, the differential temperature approached zero in a stepwise fashion as the temperature in case 1 approached that of case 2. Decreased entrainment rate due to increased buoyancy did not allow the MLD of case 1 to remain as deep as that of case 2. This caused temperature of case 1 at day 70 to exceed that of case 2. It did not, however, exceed the increase seen in Events #1 and #2, as the difference in the MLD's between case 1 and case 2 were smaller in this event.

There was an immediate decrease in salinity in the first case, as in the first two events, as the precipitation diluted the layer. This decrease continued until cessation of the precipitation event. Mixing by entrainment decreased the differential salinity to a value of  $-0.3\text{ppm}$ , after which it rapidly approached that of case 2.

#### 4. Event #4 (Mar 1969)

Examining the MLD model output for the  $E-P=0$  case (Fig. 6 on page 22), it appears that this was the period of deepest MLD ( $\bar{h} > 100\text{m}$ ). This was also the beginning of the period of transition from the colder winter regime to the warmer summer regime. Here the MLD began to shallow due to decreasing wind speed and  $Q_0 > 0$ .

This event provided different results than Events #1 to #3, and Fig. 9 on page 30 is presented for better resolution. As in the previous events, there was an initial decrease in both the differential MLD and in temperature (point a). This was associated with the precipitation event and a large decrease in  $U$  from  $18.0$  to near  $0.0\text{ m/s}$ . During this shallowing period there was a slight wind increase causing  $U$  to peak to  $5.0\text{ m/s}$ , and a deepening in both case 1 and case 2. This was less in case 1 than in case 2. This differential in MLD generated a positive differential temperature (point b). The positive differential temperature immediately decreased as the wind dropped to zero, and the MLD became very small, order  $1\text{ m}$  (point c). Net heat loss cooled the upper layer in case 1 more than in case 2, generating a severe negative spike in the differential temperature ( $\sim -0.10^\circ\text{C}$ ). A series of mild wind speeds until day 98 yielded various negative and positive peaks in the differential MLD's and temperatures.

At day 100 a strong wind ( $U \sim 8.0\text{m/s}$ ) returned the MLD in case 1 equal to that of case 2, making the differential MLD zero (point d). This mixing decreased the differential temperature to near zero, but it remained slightly colder as the entrained water from below the mixed layer remained warmer than water of the previous shallow layer.

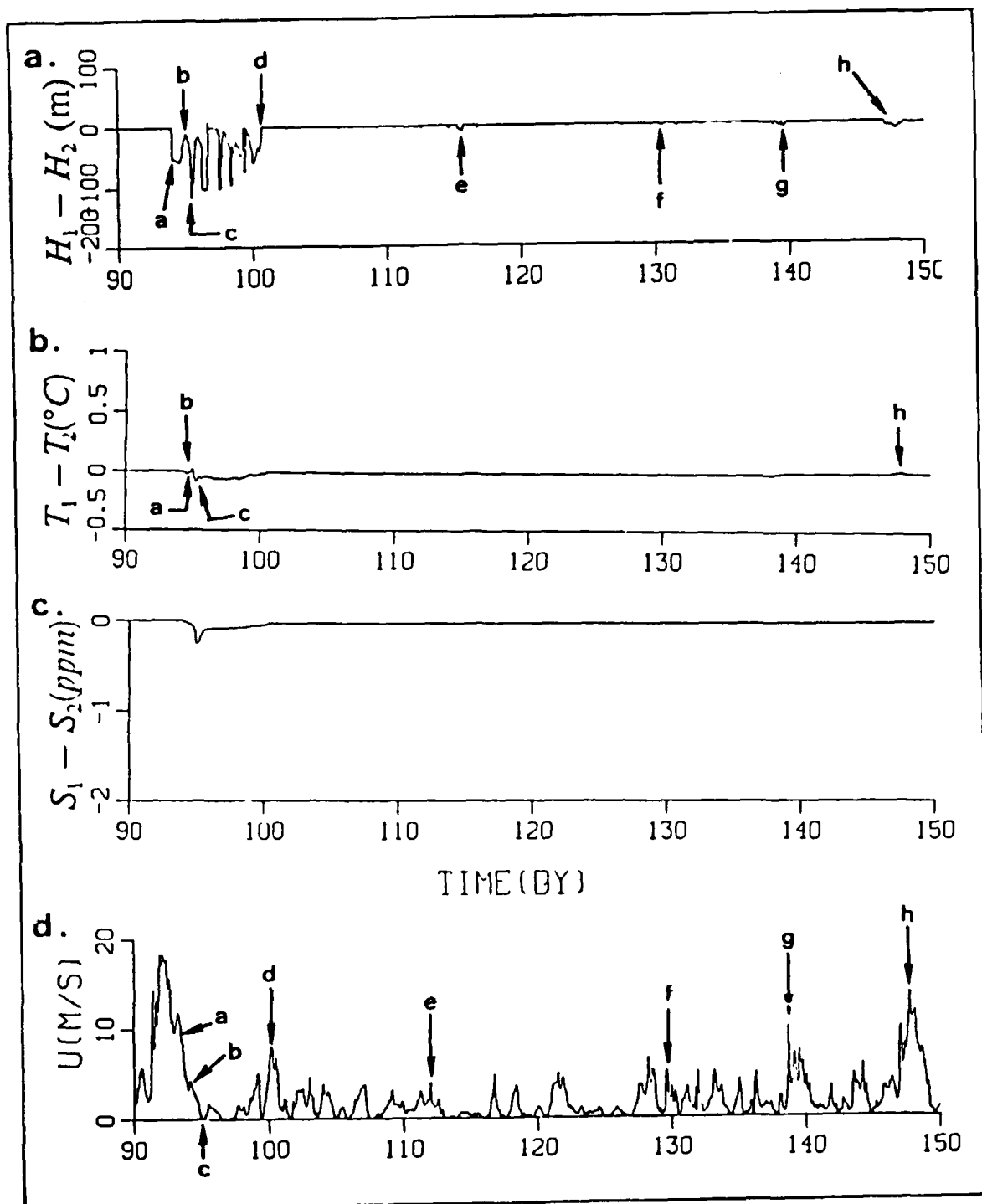


Fig. 9. Event #4 (Mar 1969): (a) differential MLD, (b) differential temperature, (c) differential salinity, and (d) wind speed

Strong winds at days 113, 130, and 140 continued entrainment, thus, diffusing the colder layer in case 1 with the warmer water below, and bringing the differential temperature closer to zero (points e to g).

Near the end of this 60-day experiment there was a very strong mixing event at day 147, induced by a  $U$  peak of 15.0 m/s with a duration of 3 days. Almost 60 days after the single precipitation event, there was still an effect on the mixed layer. Examining the differential MLD and temperature, it appeared that the MLD in case 1 did not deepen as much as in case 2. This deeper MLD caused the temperature in case 1 to begin to exceed that of case 2 (point h).

Following the cessation of precipitation, in the first case, diluted salinity was mixed by entrainment, decreasing the differential salinity to a value of -0.4ppm. After this it rapidly approached that of case 2 by wind mixing.

#### 5. Event #5 (Apr 1969)

Near the end of the March study period (Event #4) the winds decreased and the MLD shallowed (Fig. 6 on page 22). After the wind speed lull from day 123 to day 127, there was a steady rise in wind to the peak value at day 147 of  $U \sim 14.0\text{m/s}$ . This gradual increase provided the TKE to mix the layer to the deepest point for the year ( $h \sim 125.0\text{m}$ ). This was followed by a period of shallowing, induced by an abrupt fall in wind speed (Fig. 10 on page 32). The value of  $Q_0$  was positive and increasing. net heat flux. This served to provided a net heat gain in this summer regime, as opposed to the heat loss that occurred with the winter regime.

Fig. 10 on page 32 demonstrated the initial decrease of MLD in case 1, to be greater than that of case 2 (point a). Due to the low wind speeds coincident with the initiation of the precipitation event, the mixed layer of case 2 was also relatively shallow ( $h \sim 27.0\text{m}$ ). Thus the increase in the differential temperature was less than that of one day later (at point b) following a wind-driven deepening event. This produced a large decrease in the differential MLD. A series of shallowing and deepening events followed and were associated with differential temperature adjustments. This brought the differential MLD and the differential temperature back toward zero.

The largest decrease in differential salinity in Fig. 6 on page 22 occurred in this event. In this event the precipitation event was initiated after a long period of low winds, providing a shallow MLD prior to onset of the precipitation event. This may have been an unrealistic example. Given that increased wind speeds generally accompany large precipitation events like that of day 124, this hypothetical event would

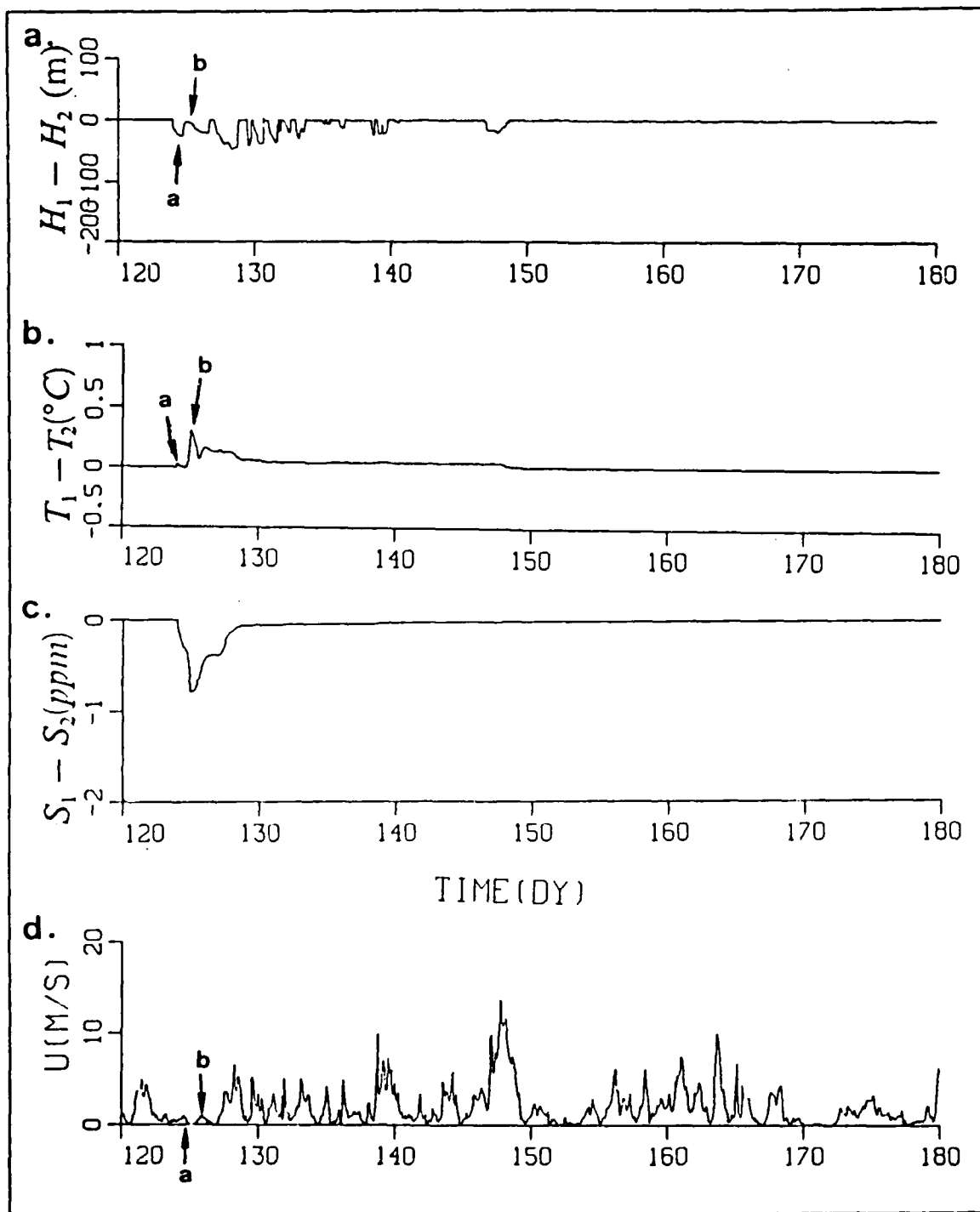


Fig. 10. Event #5 (Apr 1969): (a) differential MLD, (b) differential temperature, (c) differential salinity, and (d) wind speed



have been unlikely to occur, but it permits an interesting examination of model dynamics.

#### 6. Event #6 (May 1969)

Between day 150 and day 180 the MLD in case 2 was similar to that of Event #5, but more shallow. This shallowing was the result of decreased wind forcing as seen in Fig. 6 on page 22. Net heat gain to the ocean surface continued to increase as summer approached, and some of the largest net downward heat fluxes occurred during this period ( $Q_{0\max} \sim 700W$ ).

The dynamics of this event resembled those of Event #5. No 60-day period figures were provided. Fig. 6 on page 22 provides adequate resolution. As before, there was an initial shallowing producing a positive differential temperature associated with the shallower MLD and the summer heating regime. Until day 165, the differential MLD and the differential temperature resembled those of the previous events. After day 165, however, the resulting differential temperature profile differed from those of the previous events. Here, the differential temperature reached a post-precipitation minimum value of  $0.05^{\circ}C$  and continued to increase slowly through the rest of the study period.

This steady increase in differential temperature, when compared with the temperature plot of the mixed layer, indicated that the mixed layer was warming faster for case 1 than case 2. The MLD's were equal in depth during this period, so that this condition could not have been due to case 1 being shallower than case 2. The possible causes were decreased  $H'_{\epsilon}$ , due to decreased salinity, and/or increased  $\Delta T$ . An increased  $\Delta T$  could be caused by the mixed layer in case 1 being warmer than that of case 2, and the temperature of the water mass below being the same for both cases. If so, in the summer regime this steady increase in the differential temperature would appear to have been "self-perpetuating."

There was an immediate decrease in salinity in the first case, as in the other events, as the precipitation diluted the layer. This decrease continued until cessation of the precipitation event at day 156. Mixing by entrainment decreased the differential salinity to a value of  $-0.3\text{ppm}$ , after which time it rapidly approached that of case 2.

#### 7. Event #7 (Jun 1969)

Though the MLD for case 2 began relatively deep ( $h \sim 70m$ ) it decreased to the shallowest mean period value ( $\bar{h} \sim 20m$ ). This was caused by an initial wind event at day 181 ( $U \sim 6m/s$ ), and followed by a relative lull from day 182 to 205. Another wind

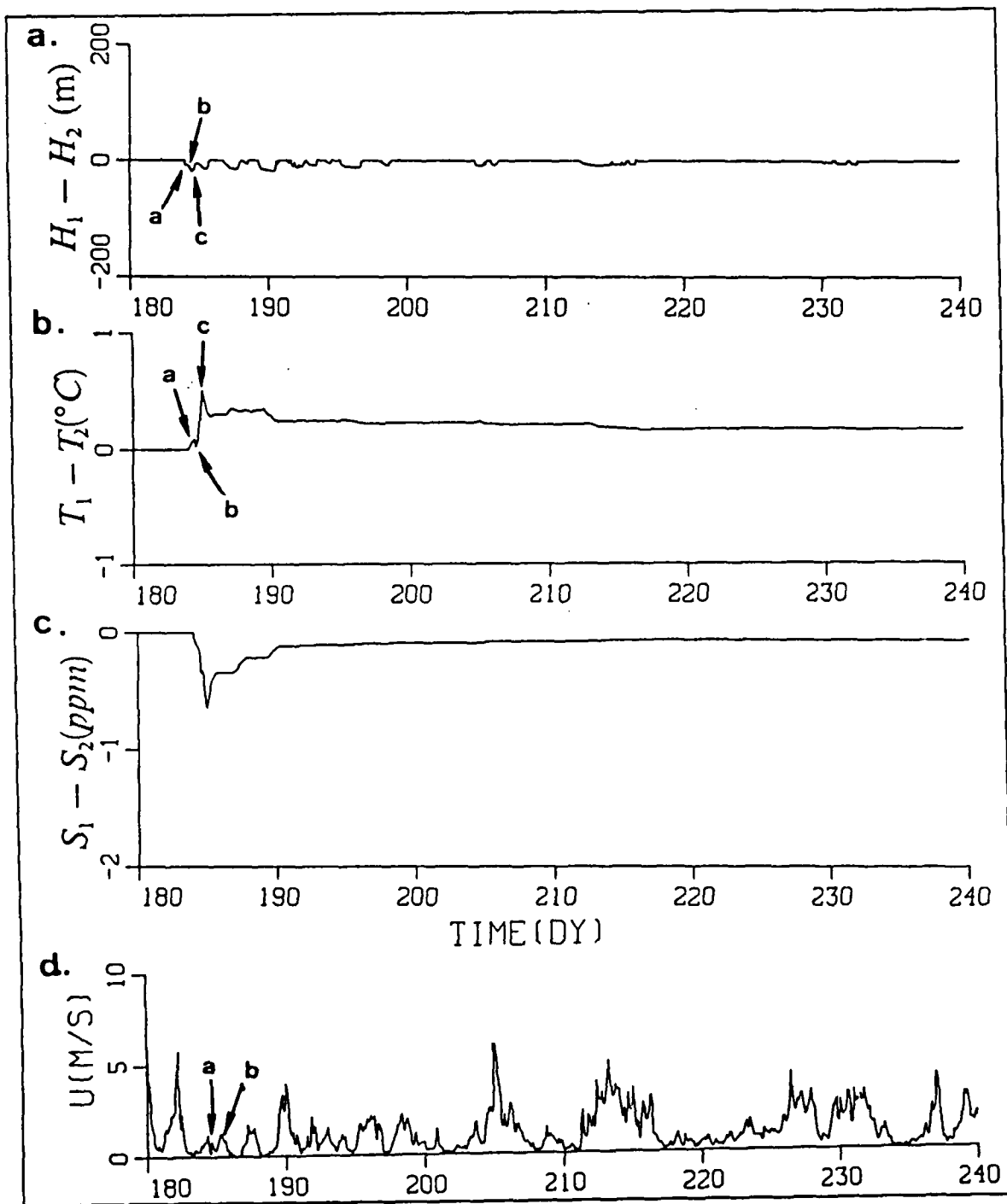


Fig. 11. Event #7 (Jun 1968): (a) differential MLD, (b) differential temperature, (c) differential salinity, and (d) wind speed

increase occurred, similar in magnitude to the first at day 205 (Fig. 11 on page 34). The net heat flux remained strongly downward, but not as strong as in the previous study (Fig. 7 on page 23).

Initially, the MLD for case 2 was shallow ( $h_2 \sim 11m$ ). At the beginning of precipitation, the MLD of case 1 shallowed to only 3m, yet there remained a small differential MLD, producing a small differential temperature  $< 0.1^\circ C$  (Fig. 11 on page 34, point a). This difference decreased with continuing low level winds which acted to deepen the MLD in both cases and yielded a decrease in the differential temperature to near zero (point b).

The most significant deepening event of this period then occurred (point c), which produced the largest differential temperature of the period ( $\sim 0.5^\circ C$ ). The mixed layer of the rain case then behaved as expected, stepping differential MLD and differential temperature back toward zero. The differential temperature for this period was much larger than for the other periods studied. This appeared to be due to the very shallow MLD's achieved by case 1, enhancing the effect of the downward summer heat flux.

The shallow MLD at the onset of precipitation did yield a stronger than normal differential salinity ( $\sim -0.070ppm$ ). The differential salinity acted as in the previous events, returning to an equilibrium value of  $\sim -0.02ppm$ .

#### 8. Event #8 (Jul 1969)

This event coincided with a shallow ( $\bar{h} \sim 30m$ ) trend in the MLD for case 2. This was associated with low wind speeds ( $U < 5m/s$ ) (Fig. 7 on page 23 and Fig. 12 on page 36). Net heat flux appeared to be steady ( $\bar{Q}_0 \sim 180W$ ).

There was an initial positive increase in differential temperature which occurred in a stepwise manner, commensurate with the differential MLD (Fig. 12 on page 36). This occurred until wind speed decreased to zero at day 216 (point a). From day 216 to 226 (points a to b) the differential temperature remained nearly constant at  $\sim 0.065^\circ C$ , with only a slight increase in time. The MLD in case 1 equaled that of case 2 (and the differential MLD  $\sim 0$ ) in this period. This condition was similar to the slight increase which was noted in for event #6, and the physical explanation is the same.

After day 226 (point b) there was a large increase in the differential MLD and differential temperature due to a  $U$  spike of  $\sim 4.3m/s$ . This acted to cool the mixed layer of case 2 more than that of case 1 and yielded a positive increase in the differential temperature ( $\sim 0.1^\circ C$ ). The differential temperature then fluctuated around  $0.22^\circ C$  for

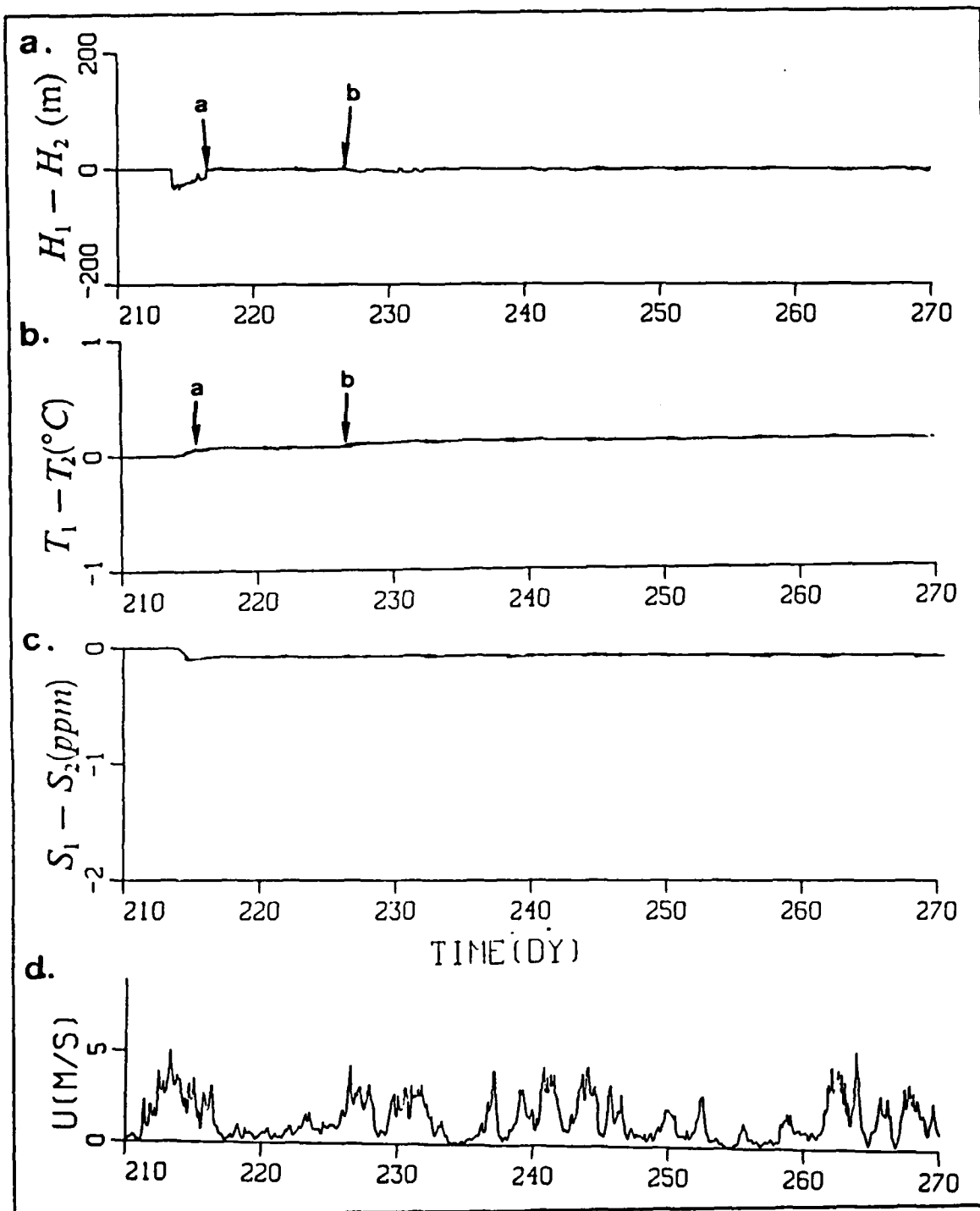


Fig. 12. Event #8 (Jul 1968): (a) differential MLD, (b) differential temperature, (c) differential salinity, and (d) wind speed

the remainder of this 60-day period as mild winds allowed shallowing of the mixed layers in cases 1 and 2 with intermittent weak spikes in wind speed producing some oscillation around this mean.

There was an immediate decrease in salinity in the first case, as in the other events, as the precipitation diluted the layer and this decrease continued until cessation of the precipitation event. Mixing by entrainment decreased the differential salinity to a value of  $-0.3\text{ppm}$ , after which time it rapidly approached that of case 2.

#### 9. Event #9 (Aug 1969)

With the exception of the initial small increase in differential temperature, this event produced results very much like that of Event #8. This small fluctuation was accounted for by the weak wind mixing ( $U \sim 4\text{m/s}$ ) occurring upon onset of precipitation.

#### 10. Event #10 (Sep 1969)

During this study period the MLD in case 2 was relatively shallow, and beginning to deepen, as there was a seasonal shift from summer to winter (Fig. 7 on page 23). This was associated with steadily increasing wind speeds (Fig. 13 on page 38). As the seasonal regime began to shift to a winter regime, the  $Q_0$  shifted from one of net downward heating toward one of cooling, although, during this period net heating remained the slightly positive.

As with the results of Event #9, these experimental results resembled those of Event #8 without the early fluctuating. In this event, prior to precipitation onset, the MLD in both cases had shallowed to near surface due to a wind speed lull from day 273 to 275 (Fig. 13 on page 38). A slight fluctuation at day 274 (point a) generated a small downward event in differential MLD ( $\sim -1\text{m}$ ) which promoted a slight upward differential temperature. With a follow on U event at day 275 (point b) of  $\sim 4\text{m/s}$ , the largest of all positive differential temperature in the twelve events was generated. This occurred along with a differential MLD of  $\sim -25\text{m}$ . Wind events followed which increasingly deepened the MLD of case 1 and brought the differential temperature back to near zero, and constantly decreasing.

This event produced the largest differential salinity of all, concurrent with this anomalous differential temperature fluctuation. Again, the very shallow MLD established before precipitation onset appeared to have contributed to this effect, and equilibrium was quickly reestablished at differential salinity  $\sim -0.01\text{ppm}$ .

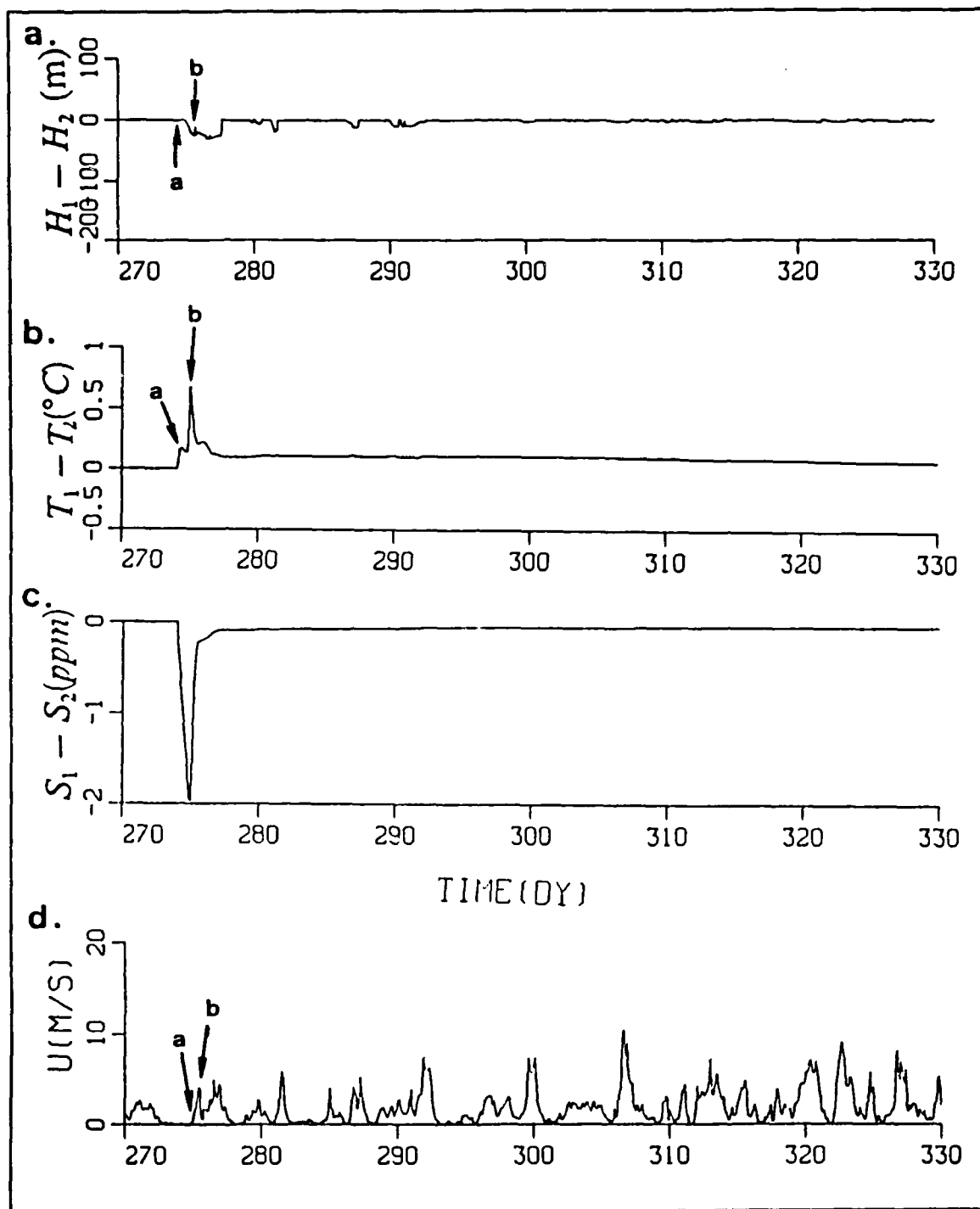


Fig. 13. Event #10 (Sep 1969): (a) differential MLD, (b) differential temperature, (c) differential salinity, and (d) wind speed

### 11. Event #11 (Oct 1969)

In this period the MLD of case 2 was becoming deep again ( $\bar{h} \sim 60m$ ) and continued to deepen in this early winter regime (Fig. 7 on page 23). Increasing wind speeds and near zero net heat values accounted for this effect.

This return to the winter regime bided a return to the differential MLD and differential temperature profiles seen in the first three events. Initial cooling of the shallower MLD of case 1 generated a negative spike in the differential temperature which moved positive as the decreased entrainment rate of case 2 inhibited entrainment of the layer. Further mixing acted to equalize MLD's and return the differential MLD and differential temperature toward zero. After the differential temperature flux moved to a positive value it remained at a larger level than observed in the first three events, as it did in the summer regimes. This indicated that the mixed layer was in transition from the summer to winter regimes and MLD's were shallower than those of the first cases.

There was an immediate decrease in salinity in the first case, as in the other experiments, as the precipitation diluted the layer and this decrease continued until cessation of the precipitation event. Mixing by entrainment decreased the differential salinity to a value of -0.2ppm, after which time it rapidly approached that of case 2.

### 12. Event #12 (Nov 1969)

This event was very similar in forcing conditions and resulting output to that of Event #11. In this event the MLD in case 2 was deeper than that of Event #11 as early winter deepening continued, and mean wind speeds appeared to be stronger with larger peak wind events (Fig. 7 on page 23). This deeper MLD yielded a larger differential MLD after precipitation onset, as well as a lesser positive peak of differential temperature. This also yielded a similar differential salinity perturbation.

## C. EXPERIMENT SUMMARY

The results of these events indicate that the effects of discrete precipitation events varied greatly as a function of low frequency seasonal heat flux forcing and higher frequency wind forcing. These two forcing boundary conditions strongly influenced the mixed layer thermal characteristics, as well as the salinity.

The average deeper, colder mixed layer in winter was significantly shallowed by a single precipitation event. This shallowing allowed for the increased loss of the thermal energy of the shallower mixed layer to the colder atmosphere, supporting a temperature decrease in the mixed layer. Wind events that followed precipitation deepened the mixed

layer, but it did not deepen as much, nor as quickly as in the case without precipitation. Follow-on wind events deepened the mixed layer until entrainment returned the MLD to that of the case without precipitation. Entrainment had a similar effect on the differential mixed layer temperature.

The effects of the precipitation event in winter were modulated by the discrete deepening and shallowing events that occurred just prior to precipitation onset. A deeper MLD increased the magnitudes of the differential values that occurred as a result of precipitation shallowing. A shallower MLD operated in the opposite sense to decrease these values. Deepening and shallowing events occurring concurrent with precipitation had a similar effect, acting to enhance or decreasing differential values.

In summer the average shallower, warmer mixed layer was less significantly shallowed by these precipitation events. Given that the mixed layer was already relatively shallow, the decrease in MLD was not as significant as in winter. Significant thermal stratification in summer yielded a large increase in mixed layer temperature with precipitation induced shallowing, as the thermal energy input at the top of the mixed layer was concentrated into a shallower mixed layer. This increased mixed layer temperature produced a more stable mixed layer as the temperature jump at the base of the mixed layer increases. The increase in temperature jump tended to further inhibit entrainment and slowed deepening of the mixed layer. Deepening slowed enough that the differential temperature actually increased with time.

The discrete precipitation events could have had a long term effect on the mixed layer. This was especially true in summer when MLD's were shallower. In cases where strong winds generated strong mixing events, the mixed layer continued to demonstrate increased buoyancy, as long as 55 days after the precipitation event, as the differential MLD became negative and differential temperature yielded a positive fluctuation.



## V. PROCEDURES, RESULTS, AND ANALYSIS

### A. PROCEDURES

The 400-day mixed layer simulation, as described previously, was conducted to examine the accumulative effect of a time series of rainfall events in explaining salinity and temperature changes with time and depth. Discrete daily precipitation data was not available for this study. Only monthly totals were available. As a result a method was devised to simulate daily precipitation values using the available oceanographic and meteorological observations. With the lack of surface pressure and upper atmospheric data, precipitation prediction became difficult, thus prediction of localized atmospheric convective activity was difficult. Utilizing wind and cloud information, however, an attempt has been made to predict precipitation associated with frontal activity. This technique was based on meteorological principles developed by Petersen (1956).

Specifically, this procedure utilized wind speed and direction, and cloud coverage data (Fig. 14 on page 42). With cloud cover data available in octaves, precipitation was allowed for cases with cloud coverage equal to or greater than 7/8. Considering pre-frontal and frontal rain, precipitation was allowed to occur for cases with wind directions from 000° (northerly winds) clockwise to 220° (southwesterly winds), and wind speeds greater than 10 kts. This accounted for the southerly to southwesterly winds that proceed a front and the "confused" northerly to southeasterly winds that accompany frontal passage. For post-frontal rain, precipitation was allowed to occur for cases with wind direction 220° (southwesterly winds) clockwise to 000° (northerly winds), and for stronger wind speeds, greater than 25 kts. This accounted for the strong southwesterly to northwesterly winds that accompany a post-frontal regime and ensured consideration of all possible wind directions. Additionally, the post-frontal case required that the sea surface temperature be greater than the air temperature, as the cold frontal air passes over warmer water. Precipitation amount was adjusted to yield the 400-day precipitation total of the observed monthly data. The resulting rain with time is contained in Fig. 15 on page 43.

This "complex" algorithm for precipitation forcing scheme was applied to the OPBL model at a range of possible amounts that may represent normal interannual variability in the North Pacific. A "medium" precipitation level was chosen by adjusting total 400-day output to equal that of the summation of the 13 month period from

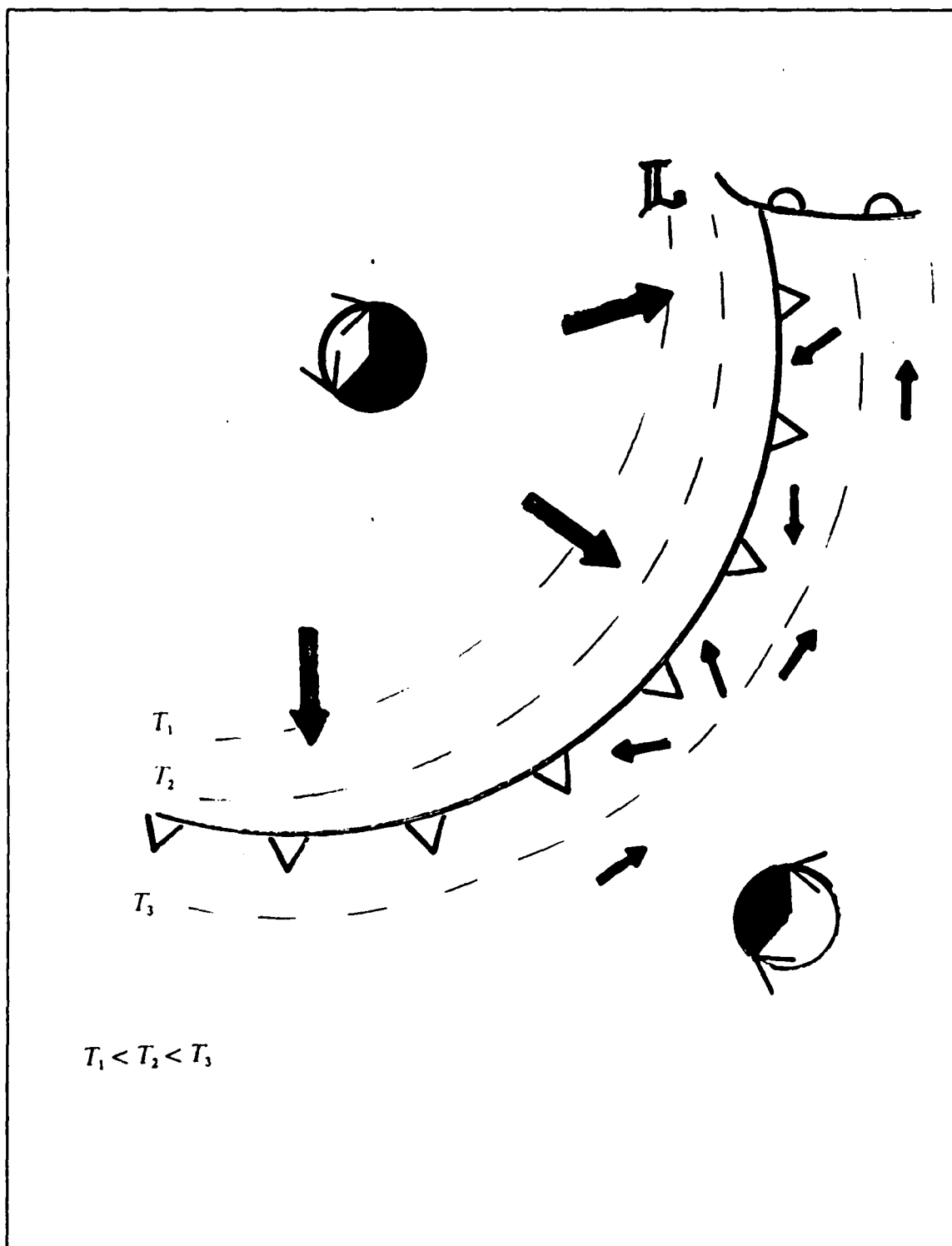
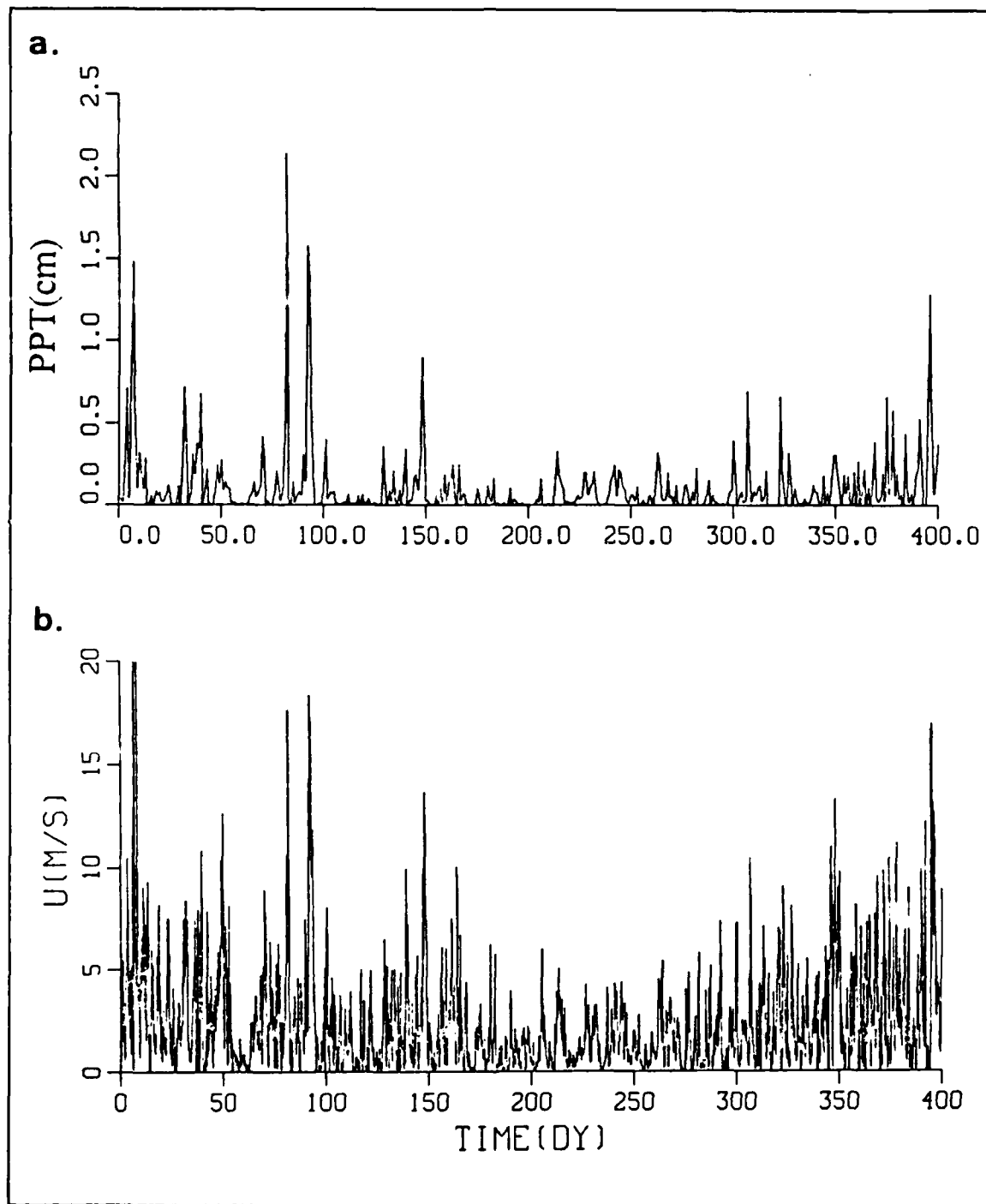


Fig. 14. Front and associated wind directions and isotherms



**Fig. 15. Complex Rain Model Output and Winds for 400 day period:** (a) rain model output for 400 days from 23 Nov 1968 adjusted to equal actual monthly totals, and (b) wind for same time period.

December 1968 to January 1970 (Table 3 on page 45). The "low" level was chosen to equal two-third's of the total 400-day precipitation total of the medium level case. The "high" level case was equal to one and one-half times the medium case and the "very high" case was made equal to three times the medium case (Fig. 16 on page 46). The same wind stress and heat flux atmospheric forcing values and initial conditions described in chapter II were used for all four model runs as in chapter IV.

**Table 2. PRECIPITATION TOTALS FOR THE 400-DAY STUDY PERIOD**

Precipitation Forcing Totals for 400-day Period	
qualitative designation	quantitative 400-day total
low	32 cm
medium	48 cm
high	96 cm
very high	160 cm

These four complex cases were compared with the effects of "simple" constant evaporation and precipitation. Here the four "simple" precipitation and evaporation rates were specified to give constant evaporation and precipitation with the same total precipitation and evaporation as those of the four complex cases. These simple precipitation cases were applied to the model so that the effects of discrete precipitation events could be compared to those of constant E-P. The resulting MLD, temperature, and salinity time series were differenced for comparison. The output mixed layer values of MLD, mixed layer temperature, and mixed layer salinity from complex and simple forcing were compared to the CTD observations.

Advection was maintained in the model at 0.0 ppm/day. Considering the placement of advection in the salinity equation:

$$\frac{\partial \bar{S}}{\partial t} = \frac{\bar{S}(E - P)}{h} + \frac{\Delta \bar{S} W_e}{h} \quad (5.1)$$

It should be noted that an increase in advection would provide the same tendency for mixed layer salinity as would decreasing precipitation.

**Table 3. MONTHLY PRECIPITATION AT OCEAN STATION "P" FOR 400 DAY PERIOD**

Monthly Precipitation for 400-day Period	
month/year	precipitation
Dec/1968	1.5cm
Jan/1969	0.6cm
Feb/1969	2.9cm
Mar/1969	3.3cm
Apr/1969	4.2cm
May/1969	3.1cm
Jun/1969	2.1cm
Jul/1969	1.3cm
Aug/1969	1.3cm
Sep/1969	3.1cm
Oct/1969	5.5cm
Nov/1969	8.0cm
Dec/1969	6.3cm

## **B. RESULTS AND ANALYSIS**

### **1. Complex Precipitation and Evaporation Forcing**

The response of the OPBL model depended upon the net precipitation for the cases of complex precipitation. The 400-day total precipitation was increased from low to very high as indicated in Table 2 on page 44. An increase in total precipitation caused a general decrease in MLD's, as a result of increased buoyancy and decreased entrainment (Fig. 17 on page 47). As the precipitation level for complex precipitation forcing was increased from low to very high, it was larger in magnitude in winter than in summer, though the relative increase in summer was proportional to that of winter (Fig. 16 on page 46). This was due to the small amount of precipitation in summer compared to winter. This increase in precipitation in winter with increasing total precipitation increased buoyancy more in winter than in summer, yielding shallower MLD's for larger complex precipitation amounts. Additionally, the largest magnitude of differential MLD's occurred in winter (Fig. 17 on page 47 and Fig. 18 on page 48).

Associated with the differential MLD flux that accompanied increased complex precipitation levels was a change in mixed layer temperature and salinity. Differential

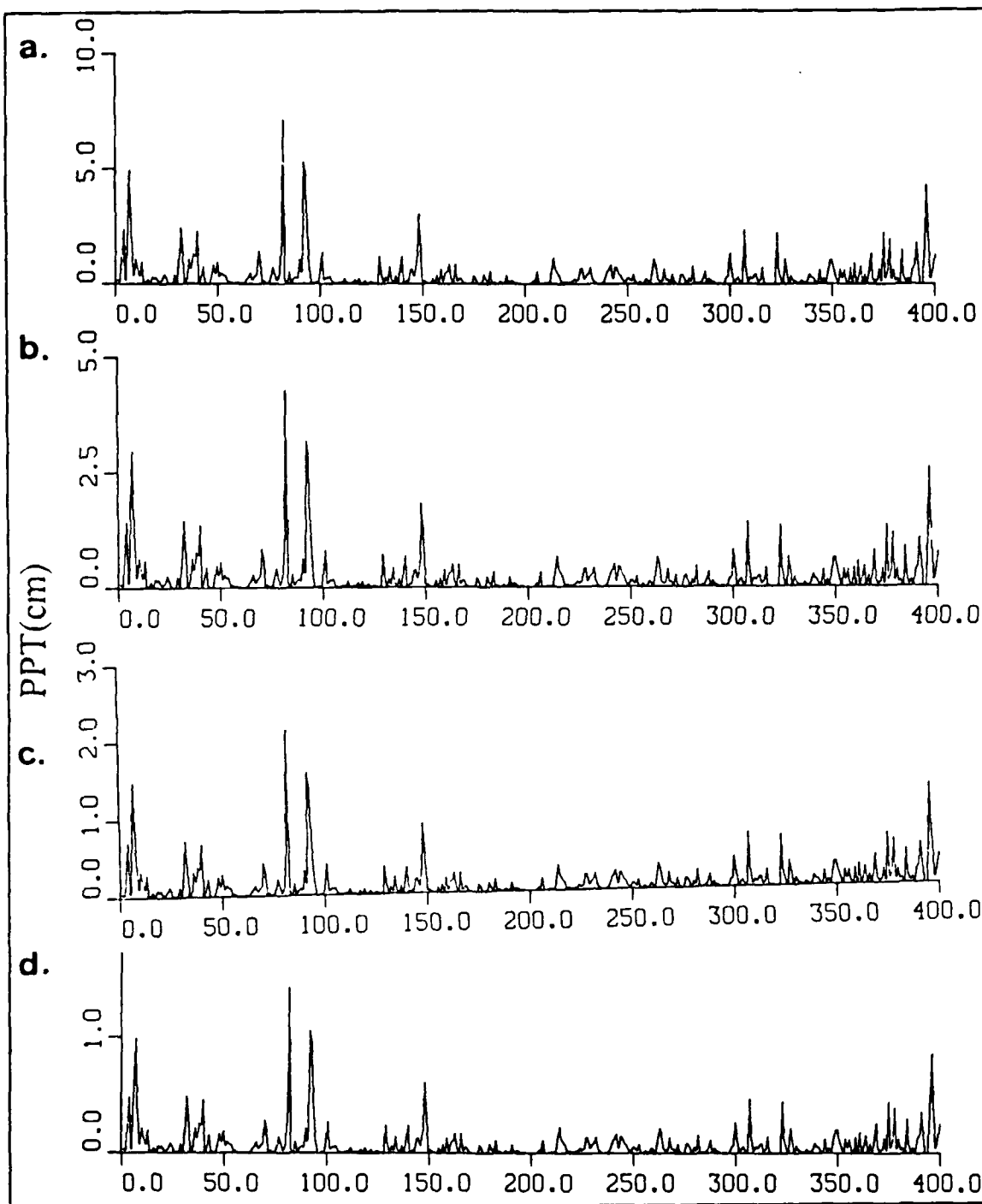


**Fig. 16. Simple and Complex Precipitation Forcing:** (a) low level precipitation, (b) medium level precipitation, (c) high level precipitation, and (d) very high precipitation.

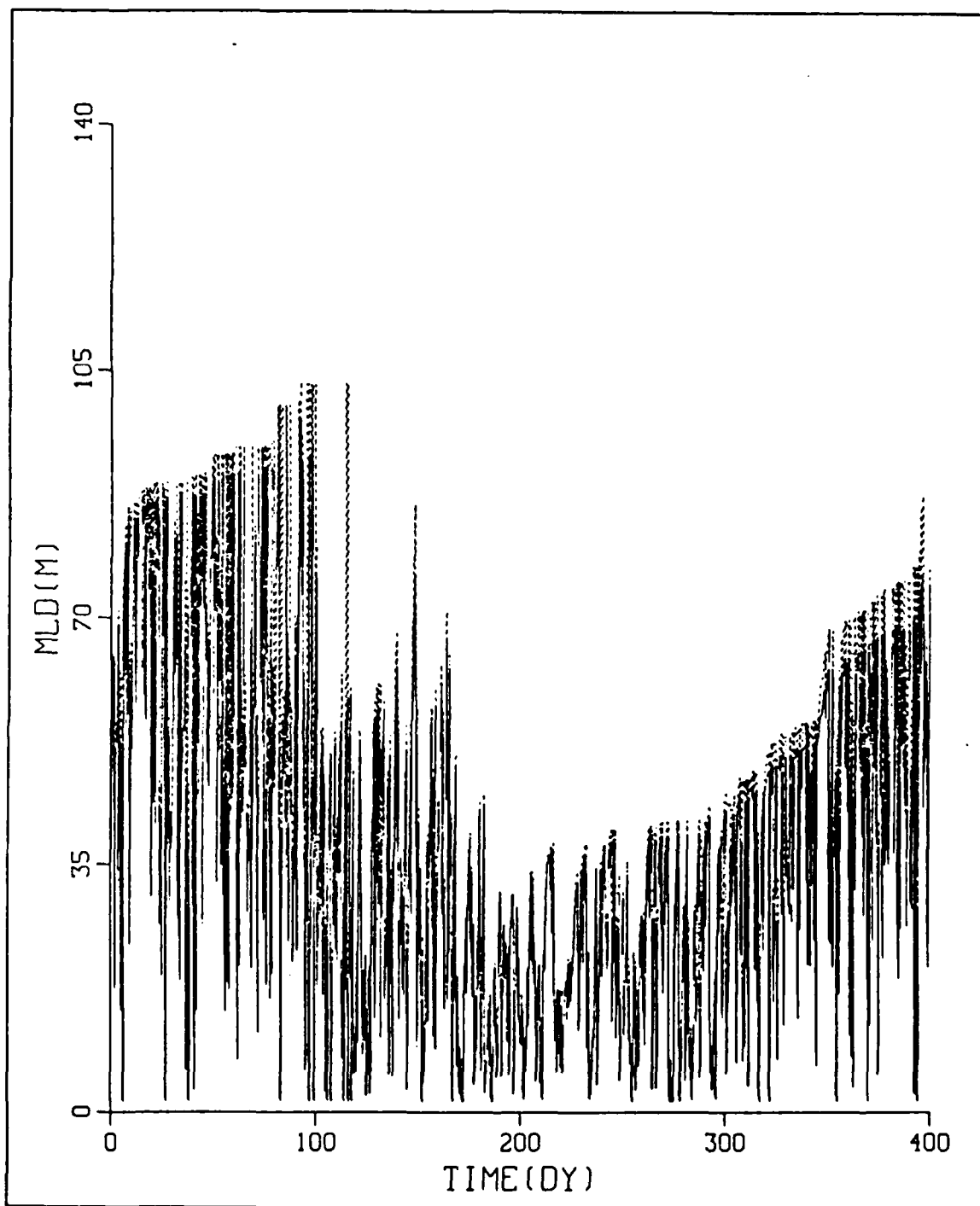
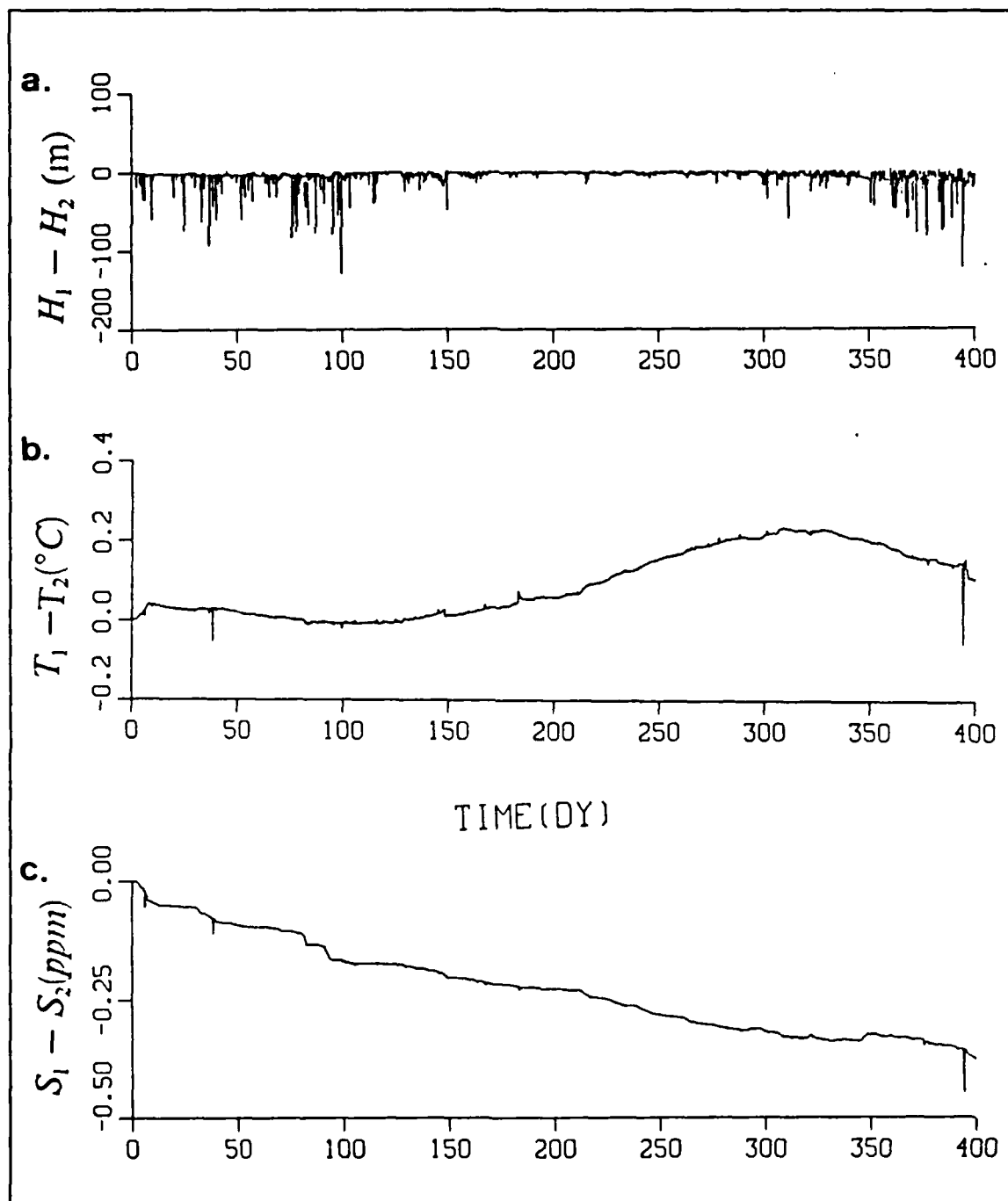
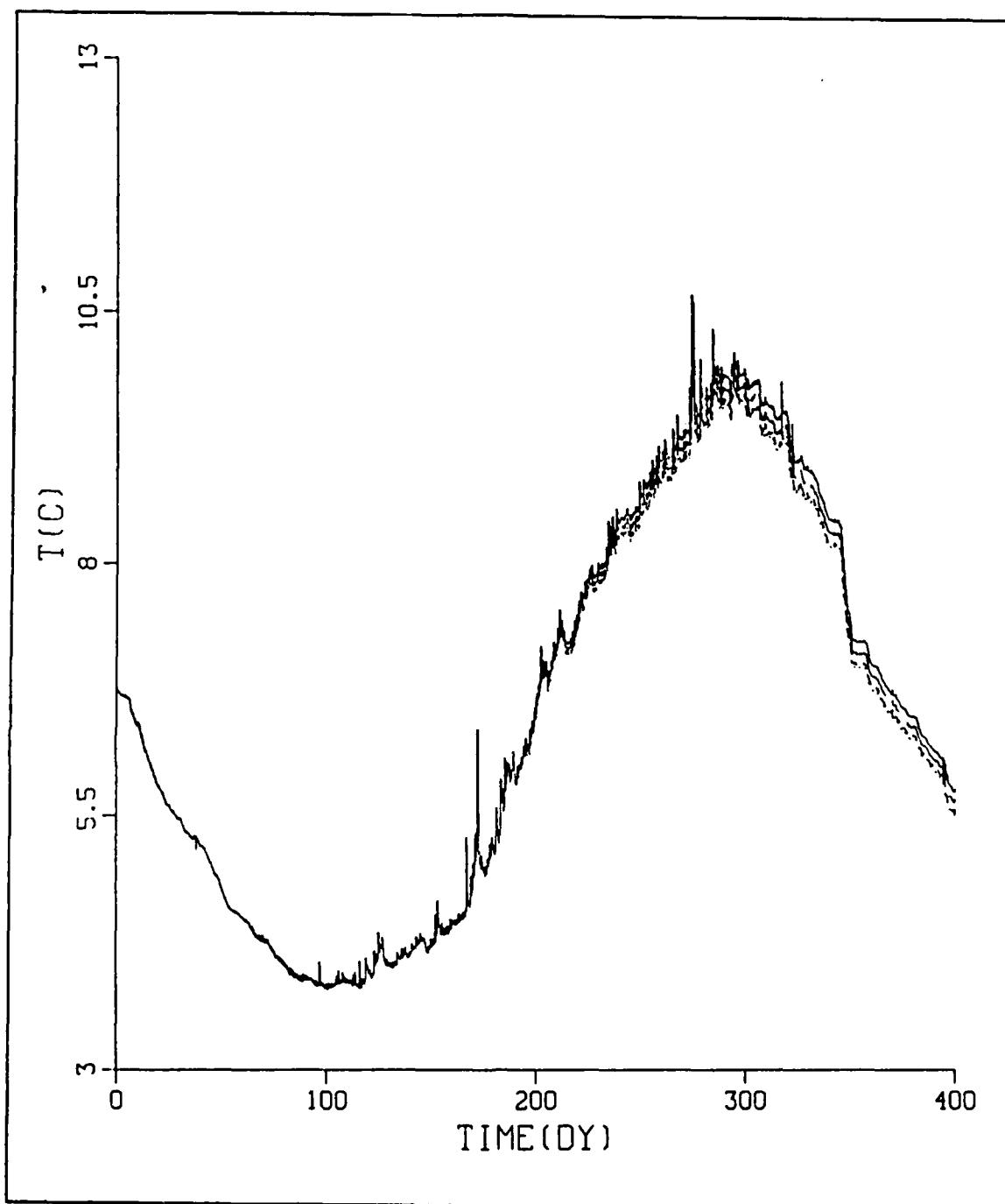


Fig. 17. Complex Precipitation Forcing Predicted MLD's: (a) solid line represents very high precipitation forced case and (b) dotted line represents low precipitation forced case.



**Fig. 18. Subtracted Values of Complex Precipitation Forcing Output:** All values are the result of subtracting Very High precipitation forcing output from Low precipitation forcing, (a) differential MLD, (b) differential temperature, and (c) differential salinity.





**Fig. 19. Complex Precipitation Forcing Predicted Temperatures:** (a) dotted line was low precipitation forced, (b) dashed line was medium precipitation forced, (c) chained-dashed was high precipitation forced, and (d) solid line was very high precipitation forced.

mixed layer temperature decreased only slightly in winter when the MLD was deep. Negative differential temperatures were induced by the winter heat loss of the shallower mixed layer. As the summer approached, and MLD shallowed due to increased  $Q_0$  and decreased winds, the differential MLD, had a more significant effect on differential temperature. Thus, the decreased MLD in the shallowing season concentrated more of the incident solar energy in a shallower layer than it would have without increased precipitation. This produced a large positive differential temperature.

Examination of the differential salinity showed a continual decrease in salinity as very high complex precipitation forcing inputted more fresh water into the mixed layer. Deepening events which yielded differential MLD's produced differing entrainment events. Deeper MLD's, characteristic of lower complex precipitation forced cases, entrained water of higher salinity than in the higher complex case. Larger precipitation events input freshwater into the surface layer inhibiting entrainment, yielding a shallower MLD. This reduction in MLD further concentrated the fresh water, reducing surface  $\bar{S}$  (Fig. 20 on page 51).

From CTD observations, actual values of MLD, temperature, and salinity were compared to those values predicted by the OPBL model with complex precipitation forcing. Verification was hindered by data voids, especially during the first 95 days of the study. Nevertheless, it may be concluded that the MLD's of the CTD data were best approximated by the model using very high complex precipitation. The envelopes of the fluctuating MLD of all four complex precipitation forcing cases appeared to be deeper than those of the CTD casts. With the small number of CTD's over any synoptic period, an hour-by-hour comparison was not possible, although MLD was predicted to fluctuate diurnally by as much as 50 m/day. As the level of precipitation was increased, the resulting MLD became shallower. Thus, the case with the largest precipitation amount appeared to most closely approximate the CTD envelope for MLD (Fig. 21 on page 52).

The mixed layer temperatures compared favorably with observations in all four complex cases. As the study period progressed, the temperatures of the actual data increased more than those from complex precipitation forcing commensurate with the actual MLD being shallower. Thus, the case with the highest complex precipitation produced the greatest shallowing, yielding the highest summer temperature. The peak temperature from the very high complex precipitation case, however, only slightly exceeded that of the low precipitation case (Fig. 22 on page 53).

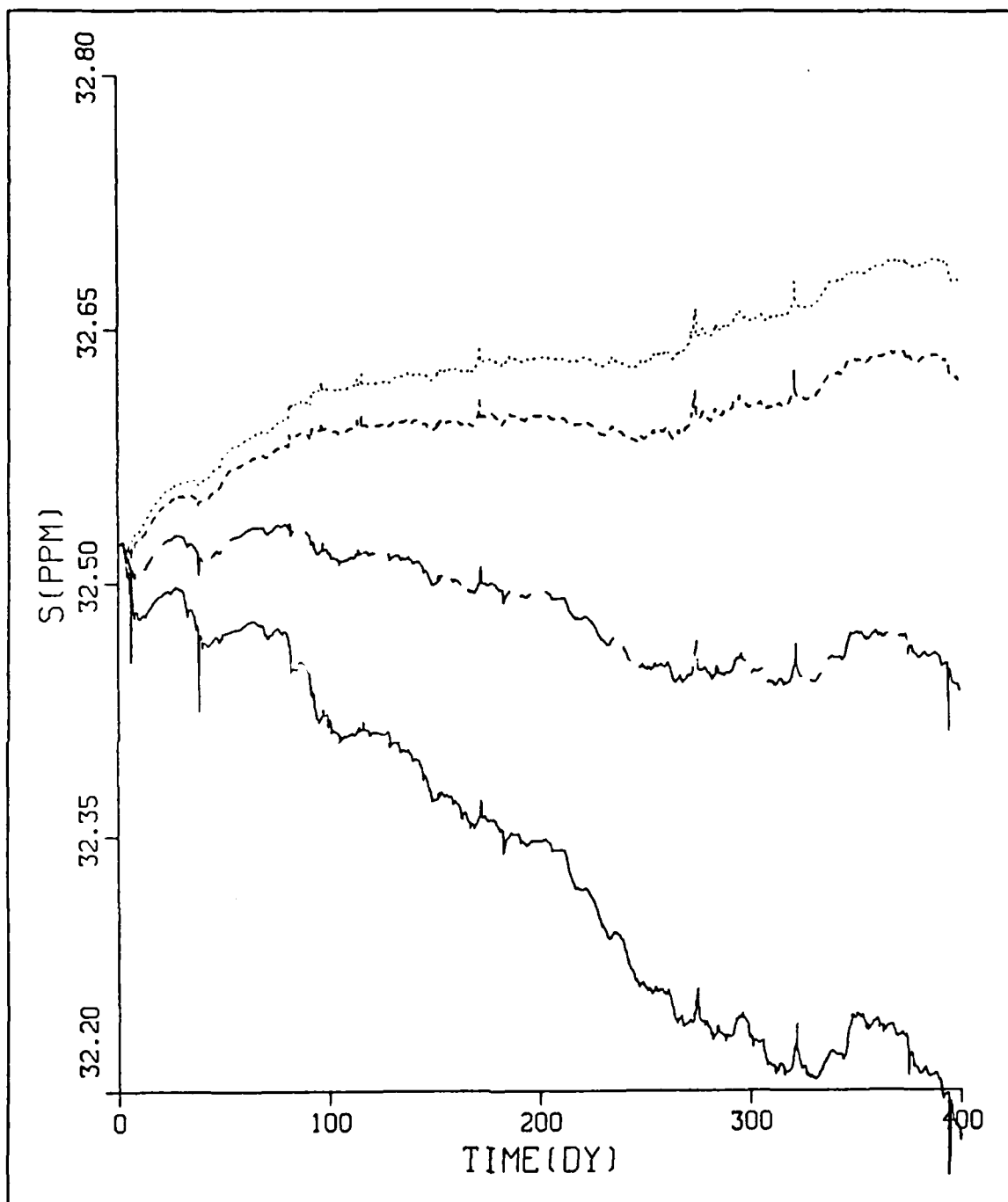


**Fig. 20. Complex Precipitation Forcing Predicted Salinities:** (a) dotted line was low precipitation forced, (b) dashed line was medium precipitation forced, (c) chained-dashed was high precipitation forced, and (d) solid line was very high precipitation forced.

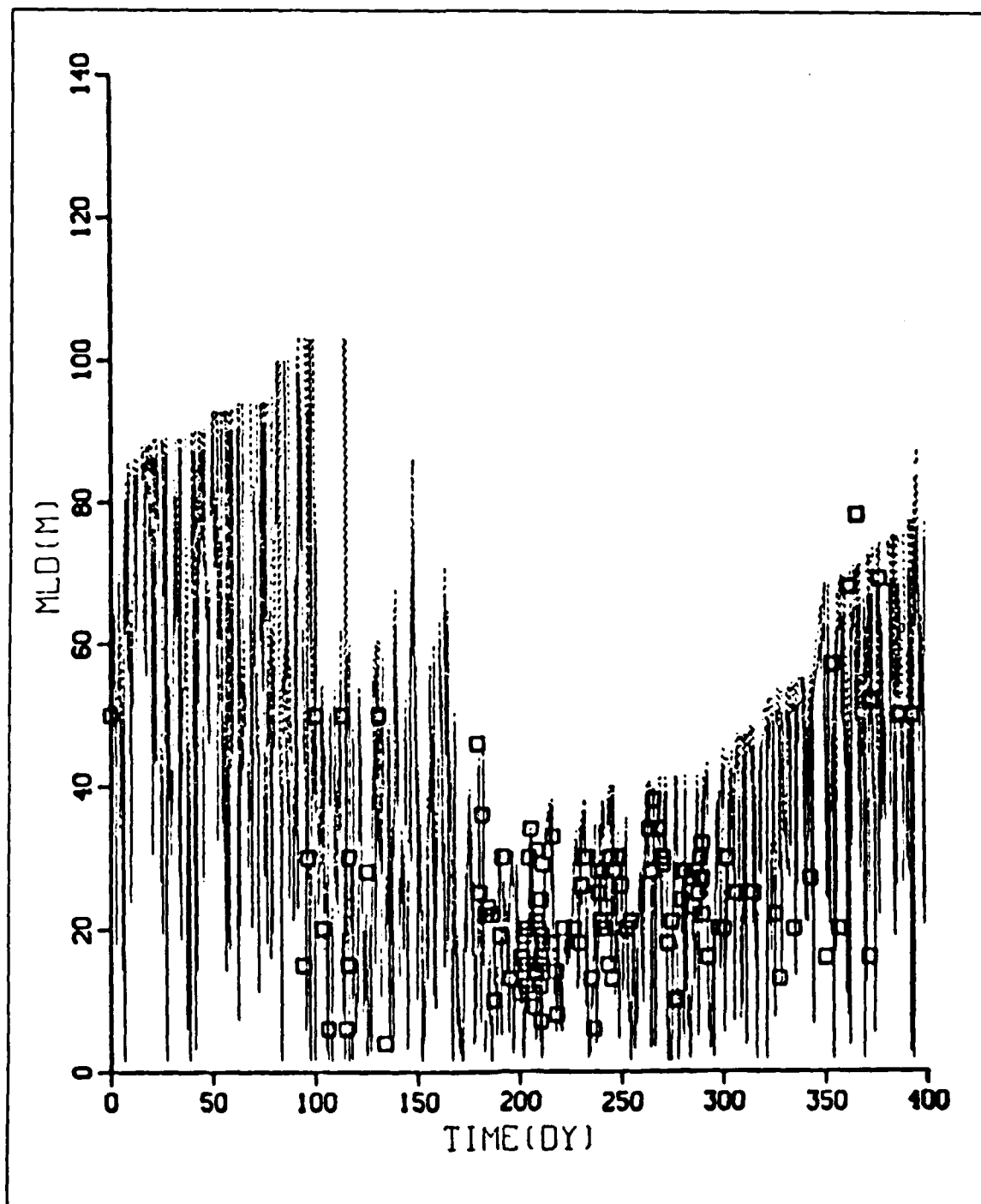


Fig. 21. Complex Precipitation Forcing Predicted MLD and CTD MLD: (a) the solid line was very high precipitation forced and (b) the dotted line was low precipitation forced.

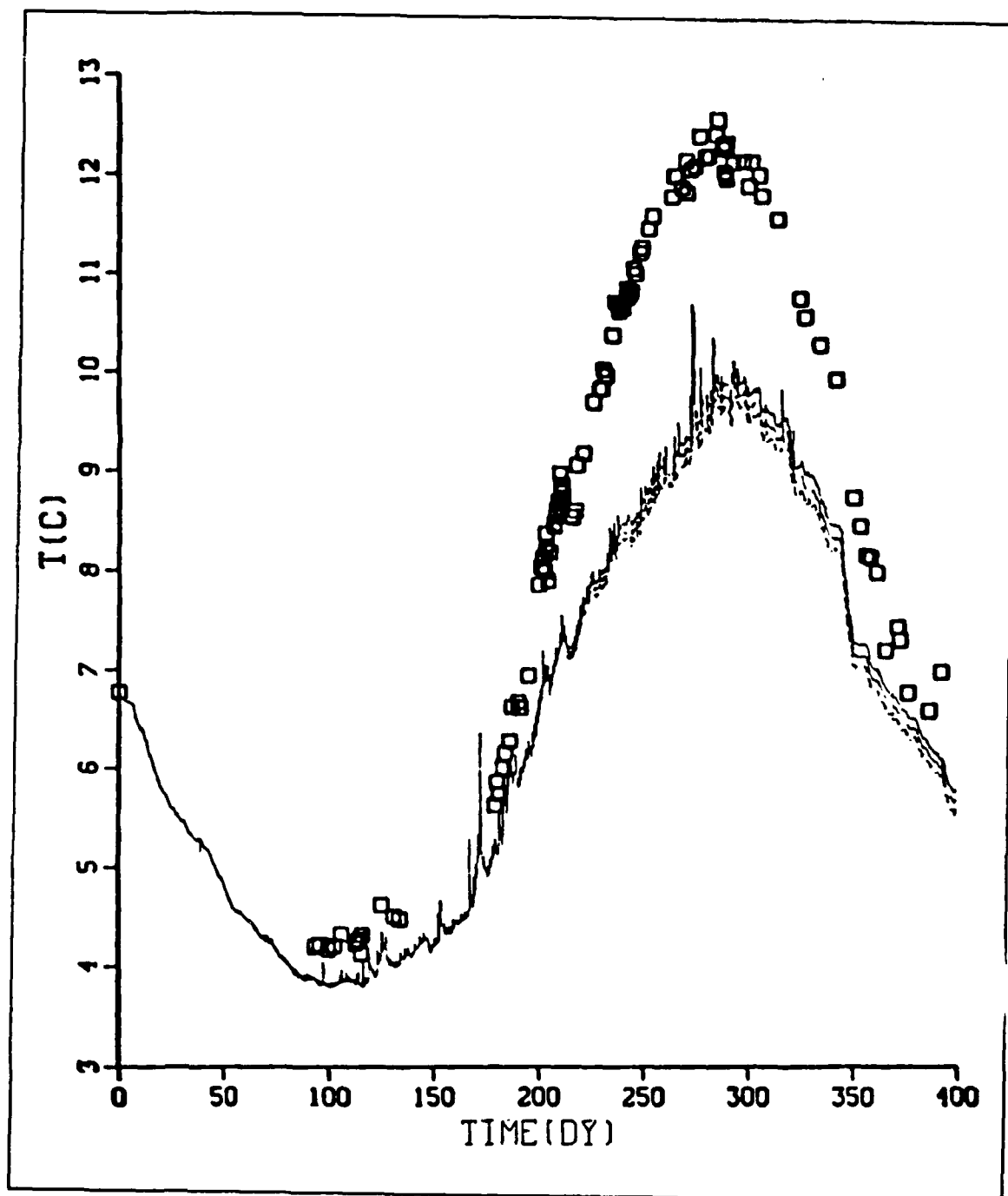


Fig. 22. Complex Precipitation Forcing Predicted and CTD Temperature. (a) dotted line was low precipitation forced, (b) dashed line was medium precipitation forced, (c) chained-dashed was high precipitation forced, and (d) solid line was very high precipitation forced.

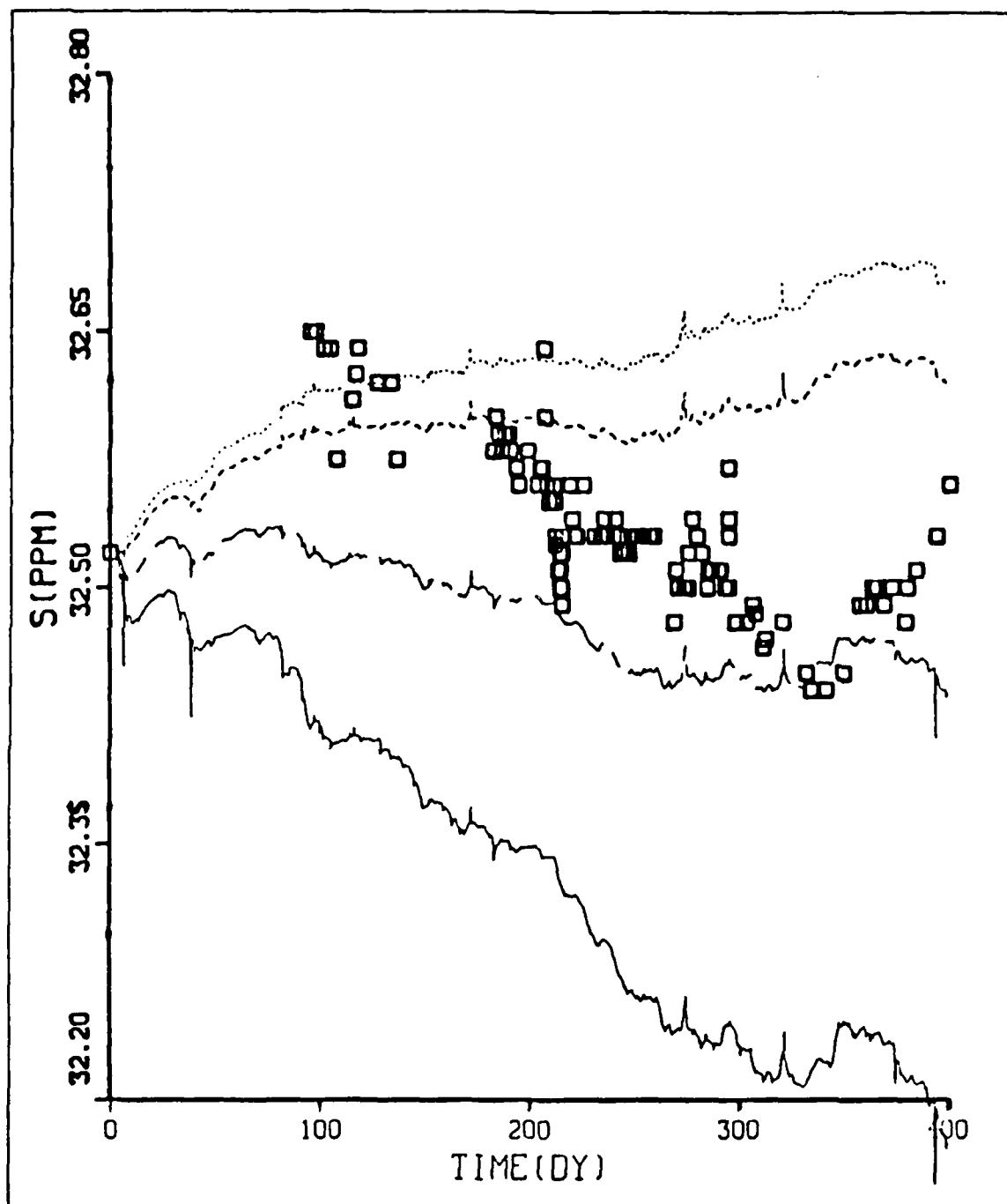


Fig. 23. Complex Precipitation Forcing Predicted and CTD Salinity: (a) dotted line was low precipitation forced, (b) dashed line was medium precipitation forced, (c) chained-dashed was high precipitation forced, and (d) solid line was very high precipitation forced.

The model-predicted salinity values yielded less certain results. Actual CTD salinity data behaved in a cyclic manner during the study period. Here the initial salinity of 32.5 ppm immediately increased with increasing MLD. As the observed MLD shallowed, the salinity decreased, until the minimum was achieved in summer. This was possibly associated with shallowing due to decreased wind and precipitation. As MLD deepened again around day 330, salinity increased (Fig. 23 on page 54).

Overall, this observed cyclic behavior was best approximated by modeling with high complex precipitation forcing. The two cases with precipitation less than the high case yielded salinity values that consistently exceeded those of the actual data, and were non-cyclic. During winter deepening for these cases, the salinity increased dramatically from day 0 to day 100. During spring shallowing and into summer, the salinity continued to increase gradually, and did not exhibit a cyclical decrease. For the very high complex case, the salinity exhibits a decreasing trend almost immediately. Here the buoyant damping of the turbulence by the strong precipitation generally countered the shear production of turbulence attributable to the wind stress.

Though the high complex precipitation case did agree with the cyclic behavior of the CTD salinity data, there were salinity observations of significant disagreement with the model prediction. As stated previously, peak salinity in winter was less than the actual value. In summer the salinity minimum was larger than the observed minimum by  $\sim 0.7$  ppm.

## **2. Constant Precipitation and Evaporation Forcing**

The results obtained during this study were similar to those for the complex precipitation forcing study. Upon comparing the various magnitudes of simple precipitation forcing, it was expected that increasing levels of constant E-P would have a magnifying effect on the mixed layer parameters. For simplicity, high and low precipitation forcing cases were compared here. The increased level of precipitation in the high case yielded a shallower overall MLD than the low case (Fig. 24 on page 56). This shallowing effect was stronger in winter than in summer, as MLD's tended to be deeper in winter. The peak predicted in the shallower period in the low case (Fig. 24 on page 56 point a) did not appear in the high case.

It appeared that winter temperatures were well verified for all simple and complex forced cases by the actual mixed layer temperatures, as the increased precipitation yielded only slightly more shallowing. In summer, however, differential temperatures

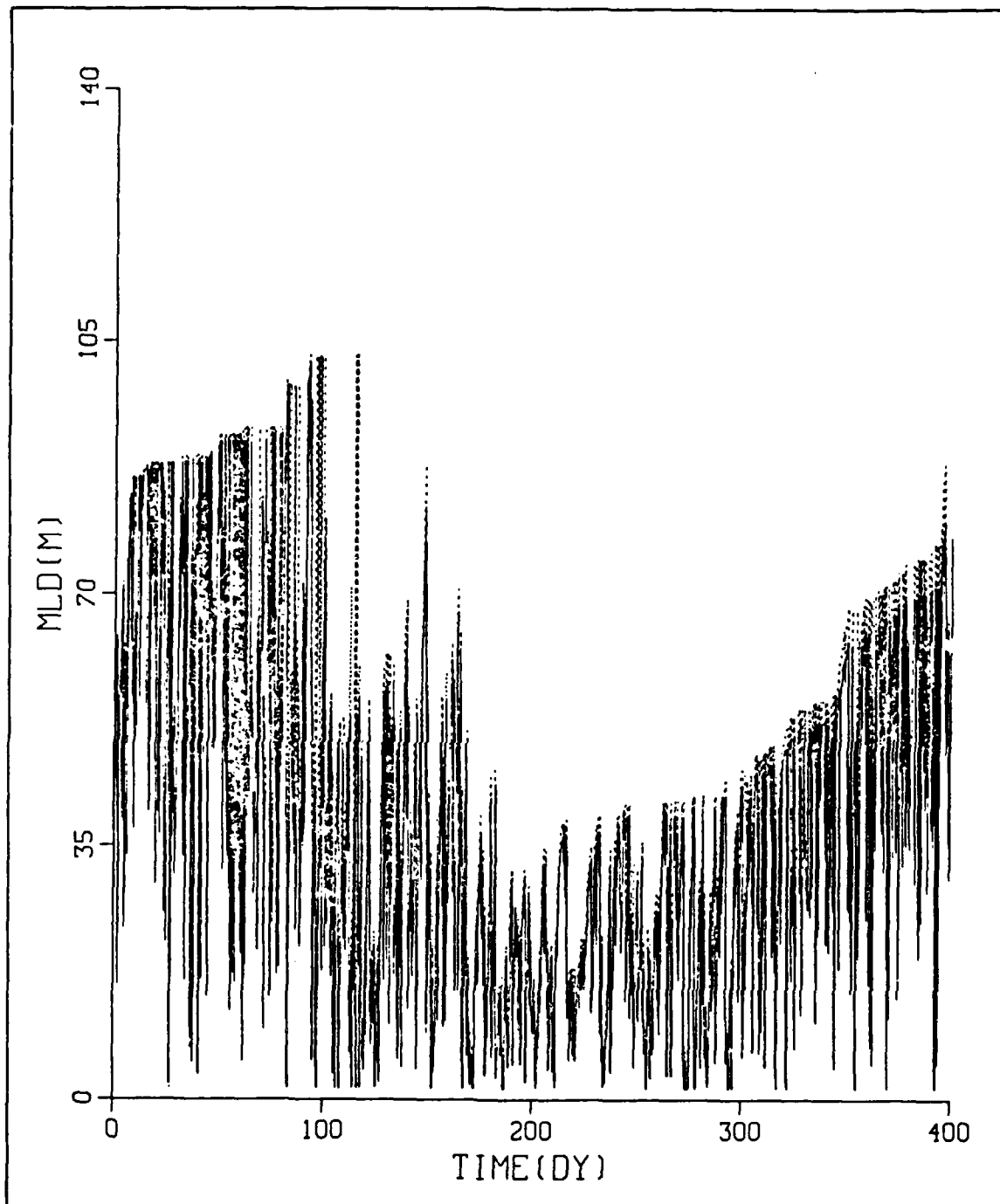
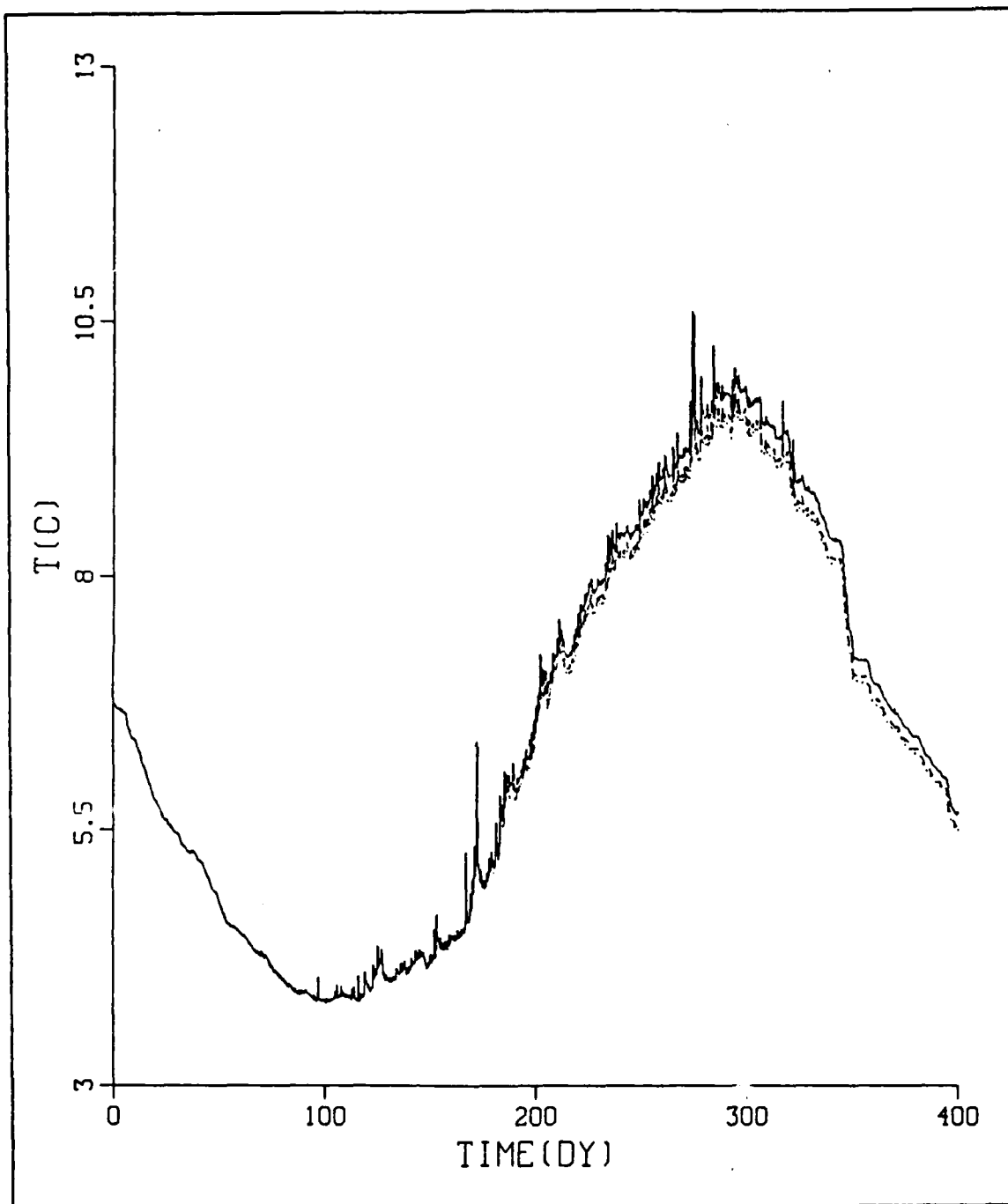


Fig. 24. Simple Precipitation Forcing Predicted MLD'S: (a) the solid line was very high precipitation forced and (b) the dotted line was low precipitation forced.





**Fig. 25. Simple Precipitation Forcing Predicted Temperature:** (a) dotted line was low precipitation forced, (b) dashed line was medium precipitation forced, (c) chained-dashed was high precipitation forced, and (d) solid line was very high precipitation forced.

increased as the high case absorbed more solar heat in a shallower layer than the low case.

As with the complex precipitation cases, the constant low and medium precipitation predictions yielded a proportional decrease in salinity. The high precipitation case proved to be the most cyclic in time over the year. The very high case yielded an almost monotonic decrease in salinity as a result of the large constant surface fresh water influx (Fig. 26 on page 59).

From comparing simple to complex precipitation forcing, it was noted that the complex case produced relatively more precipitation in winter than in summer, and there was greater evaporation in summer than in winter. The constant E-P forcing effect of the simple case thus had a larger precipitation rate during periods of no rain for the complex case (in winter when low winds occur and during the summer). In winter differential MLD fluctuated both positively and negatively about zero. It appeared to fluctuate negatively during a strong complex precipitation event yielding shallowing. It fluctuated positively during non-rain periods for the complex case, producing relative shallowing in the simple case. In winter these differential MLD values exceeded those of summer.

Differential temperature in winter showed approximately equal temperatures for the four rain levels in both the simple and complex cases. Additionally, any fluctuation in MLD had a relatively small effect on the differential temperature in the winter season. In summer a negative differential temperature was induced by precipitation being greater in the simple case than in the complex case.

With respect to salinity, differential salinity tended to be positive in winter. Here, the salinity of the complex case was usually less than that of the simple case due to the greater amount of precipitation in the complex case. It did fluctuate during this period, as periods of low winds yielded a decreased complex precipitation allowing simple precipitation to exceed it and produce a negative fluctuation in differential salinity. In summer a positive differential salinity pre-dominated. Here, the lower precipitation for the complex case allowed the salinity of this case to increase.

The very high simple precipitation case provided the best approximation to actual MLD of all study cases, both simple and complex. The large amount of precipitation produced consistently shallower MLD's than the other simple cases. Additionally, it provided shallower MLD's than occurred during the complex case when forced by low

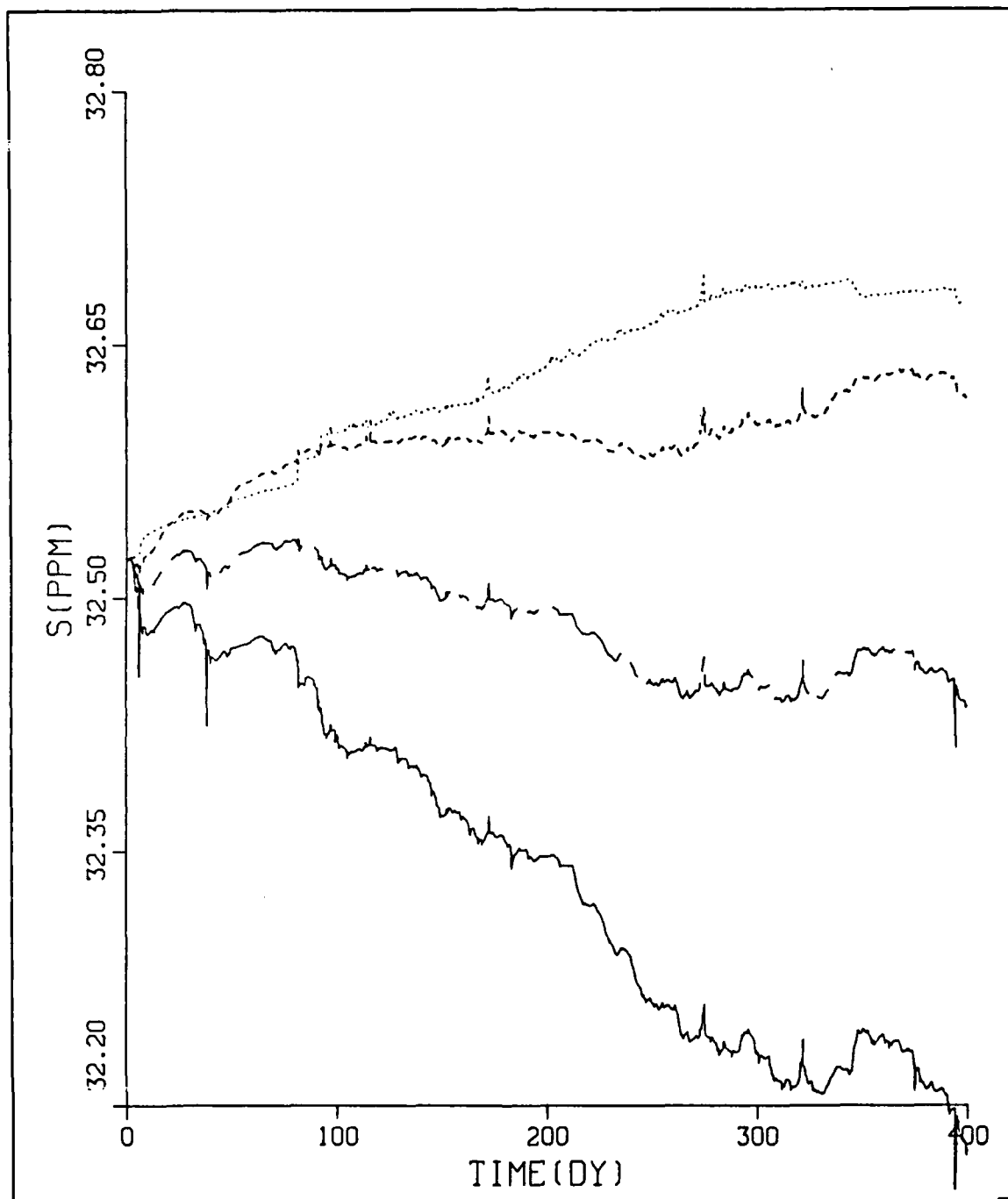


**Fig. 26. Simple Precipitation Forcing Predicted Salinity:** (a) dotted line was low precipitation forced, (b) dashed line was medium precipitation (c) chained-dashed was high precipitation (d) solid line was very high precipitation.

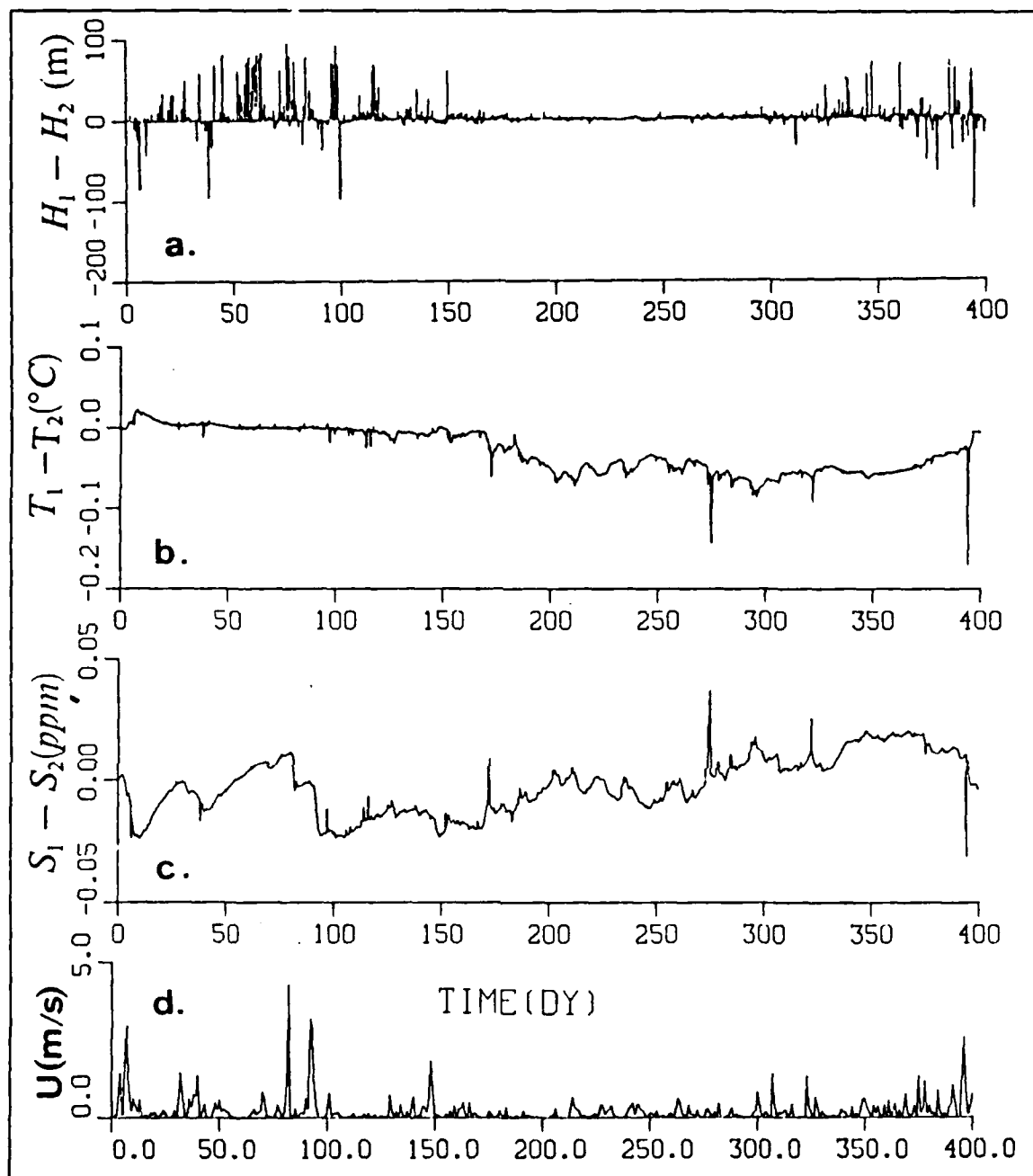


**Fig. 27. Subtracted Mixed Layer Values From High Complex and Simple Cases:** All values are the result of subtracting complex high precipitation forcing output by Low precipitation forcing, (a) differential MLD, (b) differential temperature, (c) differential salinity, and (d) complex precipitation forcing.

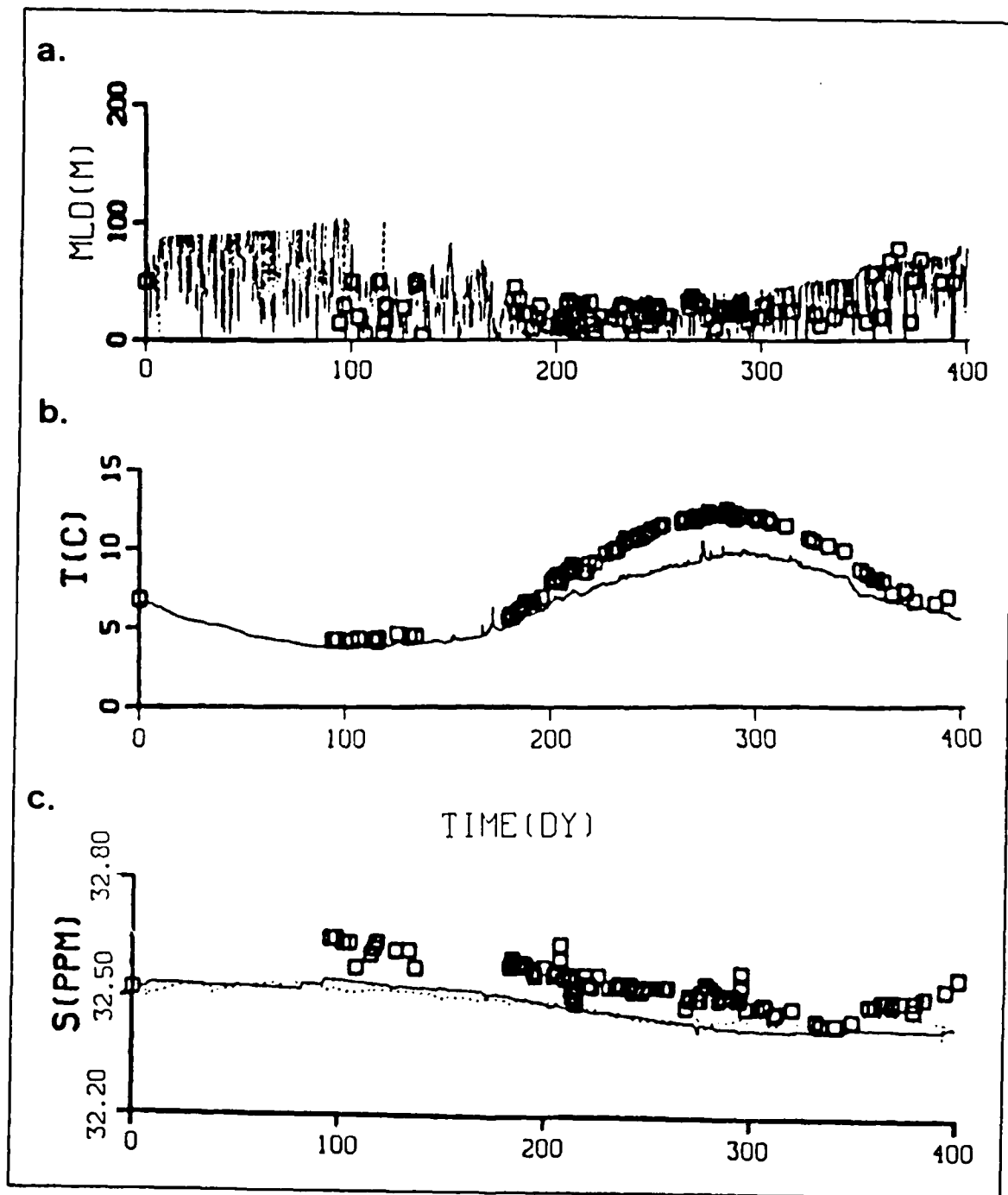


Fig. 28. Simple, Complex, and Actual Mixed Layer Values: In all three figures the solid line represents simple high forcing, the dotted line represents complex forcing.

winter winds and in all summer cases when low winds occur and MLD's tend to be shallowest (Fig. 28 on page 61).

In winter, there was close agreement between all complex and simple forced cases and actual temperature. In summer, the shallowest MLD's of the simple forced case produced the highest temperature, which though best approximated the actual temperature in summer, were still less than that of the actual case by  $2.4^{\circ}\text{C}$ .

As with complex forcing, the high simple case provided the best approximation to the actual salinity values. The simple high rain case yielded a larger negative differential salinity in winter and a lower salinity in summer than the high complex case, while still retaining a cyclic behavior with a one-year period. Its cyclic response was not as clear as in the complex case, however.

## VI. SUMMARY

This study was conducted to examine the discrete precipitation event effects on the short-term and seasonal evolution of ocean mixed layer temperature and salinity structure. Data for this study was for the years 1968 and 1969 at Ocean Station "P" located in the Northeast Pacific Ocean. Two kinds of experiments were performed:

1. the first was to simulate the response of the mixed layer to discrete (isolated) precipitation events, and
2. the second was a quasi-realistic "complex" precipitation forcing experiment, representing a realistic distribution in time of synoptic events over a 13-month period.

The hypothetical experiment was conducted using twelve separate single discrete precipitation events over a 400-day period. It examined the specific effects of a discrete precipitation event as a function of season without contamination by other complex rainfall history. This experiment showed that the effect of a single discrete rain event can vary with season and the MLD (at onset of the rain event), as well as with the intensity of the wind stress. Additionally, it showed that a single rain event can have a lasting effect on mixed layer depth and temperature for up to 55 days after the event stops.

For the main experiment a "complex" precipitation modeling scheme, producing discrete daily precipitation events from surface meteorological observations was devised and tuned to yield realistic precipitation input for the mixed layer model. The precipitation model was adjusted to give differing amounts of total precipitation. Four different precipitation "intensities" were tested: 32 cm/400-day, 48 cm/400-day, 96 cm/400-day, and 160 cm/400-day. The 50 cm/400-day case was chosen to yield the same net precipitation as the observed precipitation data. These quasi-realistic precipitation forcings were applied to the mixed layer model. The resulting values of MLD, temperature, and salinity for this 400-day period were examined by comparing them with output values when the model was forced by "simple" constant net precipitation with the same total precipitation as in the complex cases. Finally, the values predicted by the model under various precipitation forcing conditions were compared to actual CTD values.

In all study cases the MLD's approximated the MLD cycle of the actual data. The observed MLD's were shallower than predicted by the model by 10m or more. Thus, the

model runs with the most precipitation best approximated the observed MLD's. It was noted that the greatest discrepancy occurred in the first winter season of the 400-day study period. However, a large data void existed during this time period.

As with MLD, the temperatures of these studies generally approximated the temperature cycle and form of the actual data. The temperature in summer provided the greatest discrepancy in temperature magnitude with actual temperatures (exceeding those of the output data by at least  $\sim 2.5^{\circ}\text{C}$  in the complex case and  $\sim 2.5^{\circ}\text{C}$  in the simple case).

Predicted salinity provided the greatest discrepancy between the modeled and the observed cycle. Rain rates of 32 cm/yr and 48 cm/yr (that equal to the observed total) yielded salinity values which were non-cyclic and, overall, higher in value than the observations. The 96 cm/400-day case (both complex and simple) best approximated the salinity observations. Predicted salinity was less than observed in winter (by  $\sim 0.10\text{ppm}$  in the complex case and  $\sim 0.11\text{ppm}$  in the simple case) and greater than observed in summer (by  $\sim 0.07\text{ppm}$  in the complex case and  $\sim 0.07\text{ppm}$  in the simple case). The 160 cm/400-day precipitation cases produced a constant freshening of the mixed layer in both winter and summer.

In the final analysis, while the discrete precipitation events had a different effect on the mixed layer than the simple cases, the difference was slight. Increased levels of precipitation did enhance the difference between constant rain and the quasi-realistic rain cases, as seasonal differences in precipitation were amplified. The 96 cm/400-day quasi-realistic precipitation forcing case was selected as the most likely precipitation forcing for Ocean Station "P" during this time period. Despite magnitude discrepancies with observed rain at Station "P," the form and cycle of the MLD's and temperatures with respect to time were well approximated by this level of precipitation. The most important point for selection of this precipitation case was, however, the agreement with the actual salinity cycle. Here, the simple high precipitation case also approximated the shape of the salinity curve, but was not as cyclical, especially during the winter in 1969. This was probably because the complex precipitation case produced some periods without rain allowing for shallowing, and, therefore, decreased salinity. Even in winter, while the simple cases produced continuous rain. One such realistically modeled period acted to enhance cyclical behavior of salinity in the early winter of 1969, adding to MLD deepening and adding less fresh water during this period than that of the simple case.



There are several reasons why observed mixed layer temperature and salinity values may not agree with model predicted values:

1. the inaccuracies and voids in CTD data,
2. the inaccuracies in model forcing, especially in producing realistic complex precipitation forcing,
3. the inaccuracies in model initial conditions for  $T(z)$  and  $S(z)$ ,
4. the inaccuracies in representing advection, and
5. the mixed layer theory inaccuracies.

Data voids do exist in the available CTD data at Ocean Station "P." The largest data void occurred during the first 95 days of the study. At this time, there was an observation at day 0 (Nov 23, 1968) and then no observations until the 95th day (Feb 26, 1968). Additionally, data was sparse from days 95 to 180 and days 300 to 400. This would not be significant for data with small variance, as with the sea surface temperature. However, for data with strong variation such as the MLD and salinity data, the resulting analysis may be biased by lack of information at times of critical changes in mixed layer evolution.

Inaccuracies in precipitation forcing for the model may exist. Four net precipitation rates, each multiples of the first, were chosen to bracket the most realistic precipitation amounts for Station "P." The fact that the 48 cm/400-day case did not approximate the salinity cycle as well as the 96 cm/400-day case, suggests that the observed precipitation rate may be lower than the actual amount. Allen (1963) outlined the significant number of potential rain error measurement sources onboard ship at Ocean Station "P." These were:

1. the wind effects,
2. the shadowing by nearby objects,
3. the evaporation in the gauge,
4. the sea spray entering the gauge, and
5. the tilting of the gauge orifice due to roll and pitch of the ship.

Additionally, the rain model scheme used in this study was very crude. It may have inaccurately approximated the strength and duration of storm events, and would have been completely insensitive to local convection events (rain without wind). Such local convective events may account for a lower observed salinity, shallower MLD's, and higher temperatures in summer.

Inaccuracies in meteorological data used in this study to compute heat and momentum fluxes may also exist. This data was collected in 1968 and 1969, and collection techniques have improved since. In addition to the wind stress and heat flux errors introduced directly into the model by this data, these errors could produce unrealistic precipitation and evaporation events as well.

Predicting horizontal advection is difficult, and given only surface meteorological data and scattered CTD data it is not possible with any accuracy. Advective events have been known to occur at this station, as discussed in Chapter I. Such an event could greatly modify mixed layer structure. Advection was neglected for these studies, recognizing that an increase in advection of water of higher salinity has the same effect as decreasing rain and is necessary to balance the salinity budget in the longer interannual term. This was another reason for examining various rain amounts.

It is recommended that this experiment be repeated using observed discrete precipitation if possible. Alternatively, Tucker (1961) suggested a rainfall prediction scheme utilizing weather codes, using the standard international two-digit system. These follow-on studies could help answer the question as to the discrepancy in actual versus measured rainfall. Finally, precipitation from such sources as satellite imaging could be interpreted as with Hakkarien and Adler (1987) and applied to the mixed layer model.

## REFERENCES

- Allen, W.T.R., 1963: Precipitation measurements at ocean station "P." *Dept. of Trans., Met. Branch.CIR-3870. TEC-476*, pp.21.
- Camp, N.T. 1976: The role of strong atmospheric forcing events in the modification of the upper ocean thermal structure during the cooling season. Ph.D. Dissertation, Naval Postgraduate School, Monterey, CA, Dec., 175 pp.
- Denman, K.L., 1973: A time-dependent model of the upper ocean. *J. Phys. Oceanogr.*, 3, pp.173-184.
- Denman, K.L. and M. Miyake, 1973: Upper layer modification at Ocean Station "Papa:" observations and simulations. *J. Phys. Oceanogr.*, 3, pp.185-196.
- Favorite, F., et al , 1976: Oceanography of the subarctic Pacific region, 1960-1971. *Int. North Pac. Fisheries Comm.*, 33, pp.74.
- Garzon, G.H., 1987: Effects of rainfall on the seasonal thermocline. M.S. Thesis, Naval Postgraduate School, Monterey, CA, Jun., 69 pp.
- Garwood, R.W., 1977: An oceanic mixed layer model capable of simulating cyclic states. *J. Phys. Oceanogr.*, 7, pp.455-468.
- Geisler, J.E. and E.B. Kraus, 1969: The well-mixed Ekman boundary layer. *Deep Sea Res.*, 16, Suppl., pp.73-84.
- Hakkarien, I.M. and R.F. Adler, 1983: Observations of precipitating convective systems at 92 and 183 Ghz. *Met. and Atm. Physics*, 38, pp.164-182.
- Kraus, E.B. and J.S. Turner, 1967: A one-dimensional model of the seasonal thermocline. II. General theory and its consequences. *Tellus*, 19, pp.98-106.

- Miller, J.R., 1976: The salinity effect in a mixed layer ocean model. *J. Phys. Oceanogr.*, 6, pp.29-35.
- Miropol'skiy, Yn.A., 1970: Nonstationary model of the wind convective mixing layer in the ocean. *Izu. Atmos. Oceanic Phys.*, 6, pp.1284-1294.
- Paulus, A.R., 1978: Salinity effects in an oceanic mixed layer model. M.S. Thesis, Naval Postgraduate School, Monterey, CA., Mar., 77 pp.
- Petersen, S., 1956: Weather analysis and forecasting. McGraw-Hill Book Co. Inc., Vol. I, pp.189-213.
- Tabata, S., 1961: Temporal changes of salinity, temperature, and dissolved oxygen content of the water at station "P" in the Northeast Pacific Ocean. *J. Fish. Res. Bd. Can.*, 18(6), pp.1073-1124.
- Tabata, S., 1965: Variability of oceanographic conditions at Ocean Station "P" in the northeast Pacific Ocean. *J. Fish. Res. Bd. Can.*, III: series IV: June 1965, pp.367-418.
- Tucker, G.B., 1961: Precipitation over the north Atlantic Ocean. *Quart. Jour. Royal Met. Soc.*, 87, pp.147-158.

## INITIAL DISTRIBUTION LIST

		No. Copies
1.	Defense Technical Information Center Cameron Station Alexandria, VA 22304-6145	2
2.	Library, Code 0142 Naval Postgraduate School Monterey, CA 93943-5002	2
3.	Chairman (Code 68Co) Department of Oceanography Naval Postgraduate School Monterey, CA 93943-5000	1
4.	Chairman (Code 63Rd) Department of Meteorology Naval Postgraduate School Monterey, CA 93943-5000	1
5.	Prof. R. W. Garwood (Code 68Gd) Department of Oceanography Naval Postgraduate School Monterey, CA 93943-5000	2
6.	Prof. P. Chu (Code 68Cu) Department of Oceanography Naval Postgraduate School Monterey, CA 93943-5000	1
7.	Prof. R. L. Elsberry (Code 63Es) Department of Meteorology Naval Postgraduate School Monterey, CA 93943-5000	1
8.	LT M. S. Livezey, USN, SMC 1066 Naval Postgraduate School Monterey, CA 93943-5000	2
9.	Director Naval Oceanography Division Naval Observatory 34th and Massachusetts Avenue NW Washington, DC 20390	1

- |     |  |   |
|-----|--|---|
| 10. | Commander<br>Naval Oceanography Command<br>NSTL Station<br>Bay St. Louis MS 39522                                  | 1 |
| 11. | Commanding Officer<br>Naval Oceanographic Office<br>NSTL Station<br>Bay St. Louis, MS 39522                        | 1 |
| 12. | Commanding Officer<br>Fleet Numerical Oceanography Center<br>Monterey, CA 93943                                    | 1 |
| 13. | Commanding Officer<br>Naval Ocean Research and Development Activity<br>NSTL Station<br>Bay St. Louis, MS 39522     | 1 |
| 14. | Office of Naval Research (Code 1122PO)<br>800 N. Quincy Street<br>Arlington, VA 22217                              | 1 |
| 15. | Commanding Officer<br>Naval Environmental Prediction Research Facility<br>Monterey, CA 93943                       | 1 |
| 16. | Chairman, Oceanography Department<br>U.S. Naval Academy<br>Annapolis, MD 21402                                     | 1 |
| 17. | Scientific Liaison Office<br>Office of Naval Research<br>Scripps Institution of Oceanography<br>La Jolla, CA 92037 | 1 |
| 18. | Commander<br>Oceanographic Systems Pacific<br>Box 1390<br>Pearl Harbor, HI 96860                                   | 1 |
| 19. | Commanding Officer<br>Naval Eastern Oceanography Center<br>Naval Air Station<br>Norfolk, VA 23511                  | 1 |
| 20. | Commanding Officer<br>Naval Western Oceanography Center<br>Box 113<br>Pearl Harbor, HI 96860                       | 1 |

21. Commanding Officer 1  
Naval Oceanography Command Center, Rota  
Box 31  
FPO New York, NY 09540
22. Commanding Officer 1  
Naval Oceanography Command Center, Guam  
Box 12  
FPO San Francisco, CA 96630
23. Dr. T. Spence, Director 1  
Physical Oceanography Program  
National Science Foundation  
Washington, DC 20550
24. Dr. C. N. K. Mooers, Director 1  
Institute for Naval Oceanography  
Bldg. 1100, room 311  
NSTL Station  
Bay St. Louis, MS 39529
25. Director of Research Administration 1  
Code 012  
Naval Postgraduate School  
Monterey, CA 93943
26. Dr. Susuma Tabata 1  
Institute of Ocean Sciences  
Box 6000  
9860 West Saanich Road  
Sidney, British Columbia  
Canada, V8L 4B2